Cell Reports
Medicine

Article

Pyroptotic T cell-derived active IL-16 has a driving function in ovarian endometriosis development

Graphical abstract

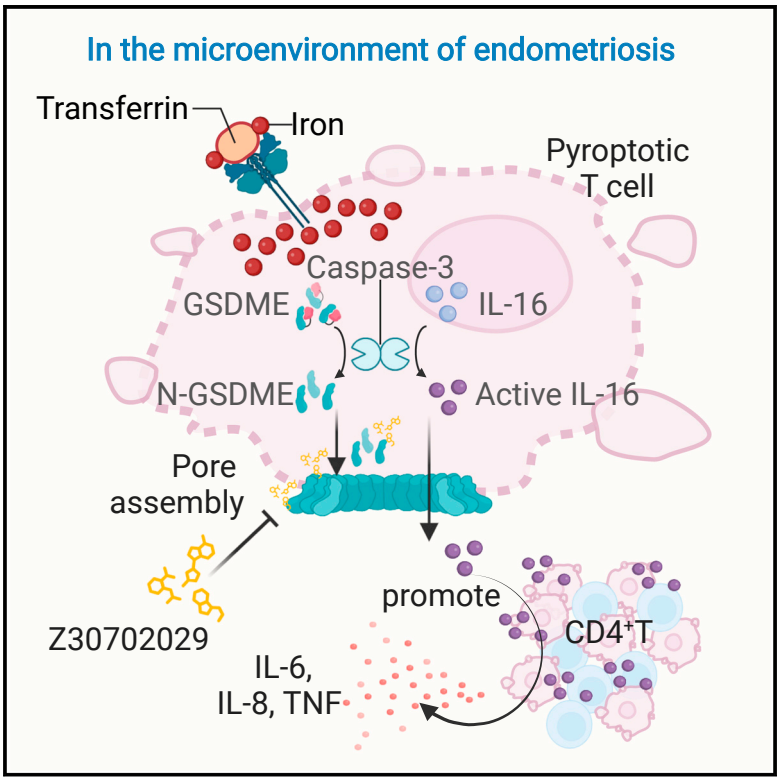

Authors

Jinghe Zhang, Weidong Zhao, Yonggang Zhou, ..., Zhigang Tian, Binqing Fu, Haiming Wei

Correspondence

victorzhao@163.com (W.Z.), fbq@ustc.edu.cn (B.F.), ustcwhm@ustc.edu.cn (H.W.)

In brief

Zhang et al. identified T cell-derived IL-16 as crucial in endometriosis inflammation, elucidating the iron-overload/caspase-3/GSDME-mediated pyroptosis axis for IL-16 release. Compound Z30702029, a GSDME-NTD inhibitor, offers promise in treating endometriosis and broader inflammatory diseases.

Highlights

- Iron-overload drives caspase-3-GSDME axis in ectopic endometrial T cells
- Caspase-3 and GSDME cooperation leads to IL-16 activation and release
- Active IL-16 has a driver function in endometriosis-associated inflammation
- Compound Z30702029 can suppress IL-16 release via GSDME inhibition

Zhang et al., 2024, Cell Reports Medicine 5, 101476
March 19, 2024
https://doi.org/10.1016/j.xcrm.2024.101476

CellPress

Cell Reports Medicine

CellPress
OPEN ACCESS

Article

Pyroptotic T cell-derived active IL-16 has a driving function in ovarian endometriosis development

Jinghe Zhang,[1,3,4] Weidong Zhao,[1,*] Yonggang Zhou,[1,3,4] Shengdi Xi,[1,3,4] Xiuxiu Xu,[1,3,4] Xianghui Du,[1,3,4] Xiaohu Zheng,[1,3,4] Weiping Hu,[1] Rui Sun,[1,3,4] Zhigang Tian,[1,3,4] Binqing Fu,[1,2,3,4,*] and Haiming Wei[1,3,4,5,*]

[1]Department of Obstetrics and Gynecology, The First Affiliated Hospital of University of Science and Technology of China, Division of Life Sciences and Medicine, University of Science and Technology of China, Hefei, Anhui, China

[2]Institute of Health and Medicine, Hefei Comprehensive National Science Center, Hefei, Anhui, China

[3]The CAS Key Laboratory of Innate Immunity and Chronic Disease, Division of Life Sciences and Medicine, University of Science and Technology of China, Hefei, China

[4]Institute of Immunology, University of Science and Technology of China, Hefei, Anhui, China

[5]Lead contact

*Correspondence: victorzhao@163.com (W.Z.), fbq@ustc.edu.cn (B.F.), ustcwhm@ustc.edu.cn (H.W.)

https://doi.org/10.1016/j.xcrm.2024.101476

SUMMARY

Endometriosis, affecting 6%–10% of women, often leads to pain and infertility and its underlying inflammatory mechanisms are poorly understood. We established endometriosis models in wild-type and *IL16*KO mice, revealing the driver function of IL-16 in initiating endometriosis-related inflammation. Using an *in vitro* system, we confirmed iron overload-induced GSDME-mediated pyroptosis as a key trigger for IL-16 activation and release. In addition, our research led to the development of Z30702029, a compound inhibiting GSDME-NTD-mediated pyroptosis, which shows promise as a therapeutic intervention for endometriosis. Importantly, our findings extend beyond endometriosis, highlighting GSDME-mediated pyroptosis as a broader pathway for IL-16 release and offering insights into potential treatments for various inflammatory conditions.

INTRODUCTION

Originally identified as a chemoattractant of T cells,[1] interleukin-16 (IL-16) exists in an inactive precursor form known as pro-IL-16. Cleavage of the C-terminal region by caspase-3 leads to the release of active IL-16.[2] Active IL-16 binds to its receptors, CD4 or CD9, exerting biological functions.[3–5] Previous research has highlighted that active IL-16 stimulates the production of proinflammatory cytokines, including IL-6, tumor necrosis factor (TNF), and IL-1β, by peripheral blood mononuclear cells (PBMCs).[6] In addition, IL-16 has been implicated in various inflammatory diseases such as sepsis,[7] systemic sclerosis,[8] malignant pleural effusion,[9] rheumatoid arthritis,[10] inflammatory bowel disease,[11] and multiple sclerosis.[12] Notably, using IL-16-neutralizing antibodies has demonstrated significant survival prolongation in animal models.[7]

Endometriosis, a widespread inflammatory disorder affecting approximately 10% of women of reproductive age globally, often leads to pain and infertility.[13–16] Ovarian endometriosis represents the most common form. This condition manifests as chronic pelvic pain (cyclical and noncyclical), painful periods, painful intercourse, and discomfort during defecation and urination.[17] The associated symptoms profoundly affect women's quality of life,[18] with inflammation being a major contributor to these manifestations.[19–26]

Numerous studies in women with endometriosis have documented alterations in the infiltration or function of various immune cells (e.g., T cells, macrophages, and natural killer [NK] T cells) and the expression of inflammation-associated factors such as IL-1β, IL-6, IL-8, IL-16, IL-33, (TNF), RANTES (regulated upon activation, normal T cell expressed and presumably secreted), matrix metalloproteinases, tissue inhibitors of metalloproteinases, monocyte chemoattractant protein-1, insulin-like growth factor-1, and neuropeptide S receptor1 in the peritoneal microenvironment.[27–35]

Several studies propose that targeting proinflammatory pathways may help alleviate endometriosis-associated pain and infertility.[17,22,27,28,36] Although the central factor initiating endometriosis-associated inflammation remains unclear, these studies suggest that targeting inflammation could offer promise in relieving endometriosis-associated symptoms. Given the role of active IL-16 in upregulating classical proinflammatory cytokines, we posit that it serves as a critical driver of inflammation in endometriosis and potentially other inflammatory conditions, including cytokine storms.

Koga et al. demonstrated elevated IL-16 levels in the peritoneal fluid of women with endometriosis.[37] Subsequent studies have identified altered genetic polymorphisms of IL-16 in endometriosis patients.[38,39] Despite the established correlation, the

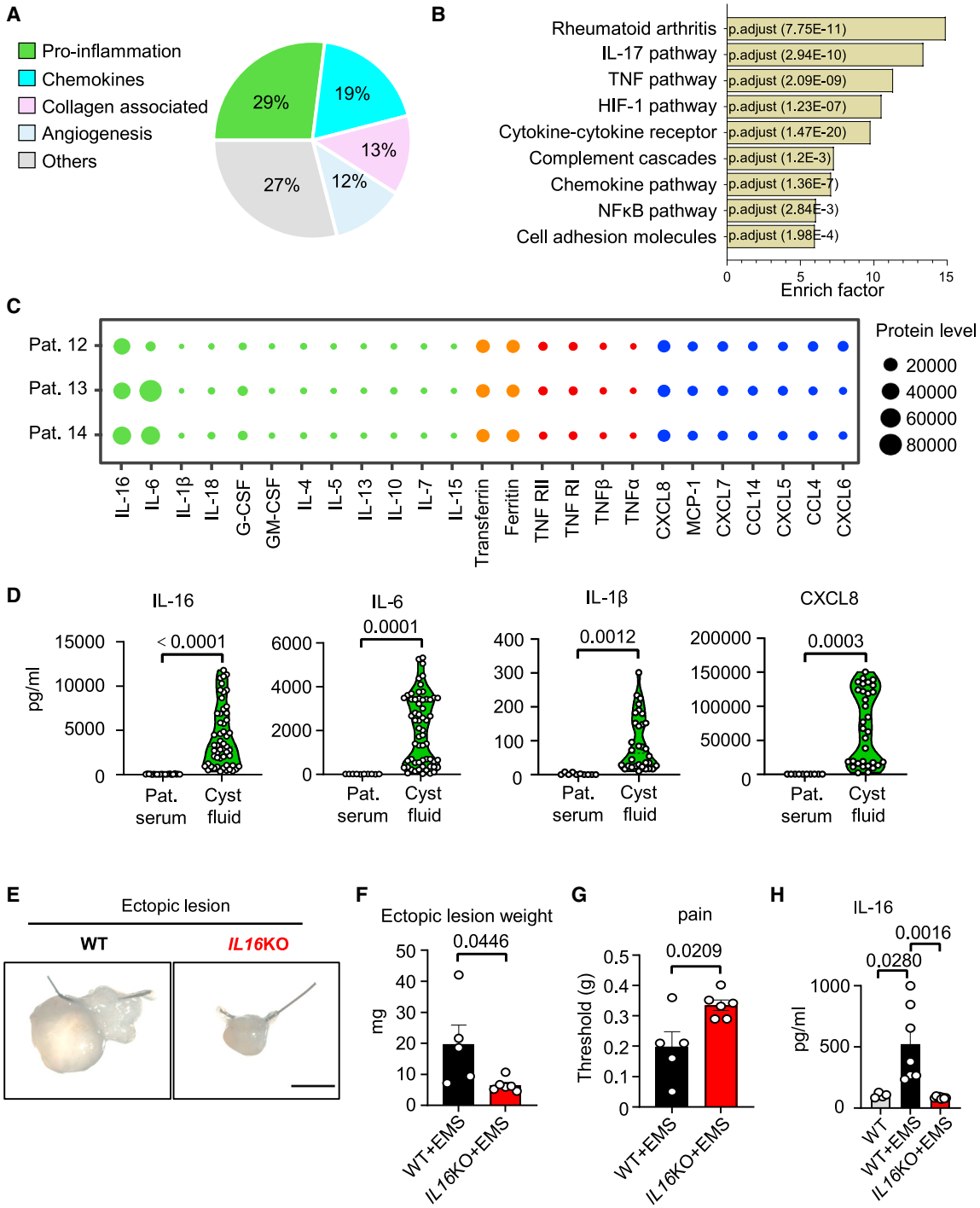

Figure 1. The crucial role of active IL-16 in ovarian endometriosis development

(A–C) Antibody microarray data sourced from cystic fluid in 3 patients. (A) Diagram illustrating the classification of cytokines with a fluorescence signal (representing the relative protein level) >2,000. (B) Enriched pathways of cytokines with a fluorescence signal >2,000. (C) Identification of relative protein levels for various cytokines in the cystic fluid.

(D) ELISA results showing the levels of IL-16 (patient serum, n = 22; cyst fluid, n = 53), IL-6 (patient serum, n = 10; cyst fluid, n = 60), IL-1β (patient serum, n = 10; cyst fluid, n = 32), and CXCL8 (patient serum, n = 10; cyst fluid, n = 32) in the cystic fluid, using an unpaired t test, data represent a pool from multiple independent experiments.

(E) Representative image of endometriosis lesions isolated from WT mice with surgically induced endometriosis and *IL16*KO mice with surgically induced endometriosis; scale bar, 2,000 μm.

(legend continued on next page)

precise role of IL-16 in the development and progression of endometriosis remains elusive.

This study delves into the immune microenvironment of ectopic endometrial tissue in ovarian endometriosis, revealing the crucial role of active IL-16 in the proinflammatory cascade underlying endometriosis pathology. Our findings demonstrate that active IL-16 facilitates the secretion of various proinflammatory cytokines, including IL-1β, IL-6, IL-8, and TNF, by binding to its receptor CD4 in the ectopic endometrial microenvironment. Moreover, we identify ectopic endometrial T cells as the primary source of active IL-16, emphasizing the involvement of the iron overload-caspase-3-gasdermin E (GSDME)-mediated pyroptosis pathway in IL-16 activation and release.

Significantly, our research led to the development of a GSDME inhibitor, Z30702029, capable of alleviating endometriotic lesion development and pain in mouse models. Collectively, these results offer valuable insights into the initiation of inflammation in ovarian endometriosis and shed light on the mechanisms involved in releasing active IL-16.

RESULTS

IL-16 is critical for ovarian endometriosis development

To identify the initiator cell types involved in endometriosis-related inflammation, we collected relatively normal posthysterectomy endometrial tissue and ectopic endometrial tissue obtained during cyst removal surgery, referred to as relatively normal endometrium (RNE) and ectopic endometrium (EE), respectively. H&E staining vividly illustrated the ovarian endometriotic tissue, showcasing endometrioid and fibrotic areas (Figure S1A). Immunohistochemistry (IHC) with anti-CD10 antibody confirmed the presence of endometrial stromal areas within the ectopic endometrial lesions (Figure S1B). Sirius red and Masson staining further validated the fibrotic regions of the endometriotic focus, characterized by type 2 collagen fibrils (Figures S1C and S1D). Surgical images revealed cystic fluid-containing foci, facilitating the categorization into "cystic fluid-stromal area-fibrotic area" for the ovarian endometriotic locations (Figure S1E). CD45 IHC indicated the presence of immune cells primarily in the ovarian endometriotic centers (Figure S1F).

Considering the structural composition of the ovarian endometriotic foci, we hypothesized that cytokines produced by endometriotic immune cells may accumulate in cystic fluid. To test this hypothesis, we conducted cytokine analysis using antibody arrays on cystic fluid samples, revealing consistent cytokine patterns across fluid samples from three patients (Figure S2A). Approximately 200 cytokines were detected among the 440 evaluated, with fluorescent signals >500 indicating protein expression. Notably, CA125, a recognized endometriosis marker, exhibited high expression in ovarian-type endometriosis, aligning with elevated CA125 levels associated with ovarian damage. Detected cytokines were related to inflammation, chemotaxis, fibrosis, growth, tumor, and iron metabolism (Figure S2B).

Using UniProt, we assigned functions and performed Kyoto Encyclopedia of Genes and Genomes pathway analysis, uncovering enrichments in its inflammation pathways such as rheumatoid arthritis, IL-17, TNF, nuclear factor κB, and chemotaxis (Figures 1A and 1B). Of particular significance, IL-16 ranked third among cystic fluid cytokines (Figures 1C and S2B). Subsequently, we demonstrated through ELISA that IL-16, IL-1β, IL-6, and C-X-C motif chemokine ligand 8 (CXCL8) exhibited higher levels in the cystic fluid compared to controls, where serum from patients was used (Figure 1D). Although IL-16 is known for promoting inflammation promotion and recruiting CD4 cells, its role in initiating inflammation in endometriosis has been unexplored.

The pivotal role of IL-16 as a central cytokine instigating inflammation associated with endometriosis was investigated using *IL16* knockout (*IL16*KO) mice, wherein IL-16 is entirely absent throughout the body (Figure S3A). Induction of endometriosis in both wild-type (WT) and *IL16*KO mice was established (Figure S3B). Comparative analysis of endometriotic lesion weight between WT and *IL16*KO mice revealed a notable reduction in the lesion weight of *IL16*KO mice (Figures 1E and 1F). In addition, an observed phenotype in *IL16*KO mice indicated a reduction in pain perception (Figure 1G). Consistent with these findings, the heightened serum IL-16 levels observed in endometriosis-afflicted mice were mitigated by *IL16*KO (Figure 1H). Furthermore, parameters such as spleen weight and IL-6 serum levels were found to be lower in *IL16*KO mice (Figures S3C–S3E). To establish a baseline comparison under naive conditions, we measured spleen weight, the number of immune cells in the spleen, and the levels of IL-6 in the serum of naive mice. These measurements confirmed that WT and *IL16*KO mice exhibited similar baselines under naive conditions (Figures S3F–S3I). Notably, T cells were slightly reduced in *IL16*KO mice. These results underscore the central and initiating role of IL-16 in the context of endometriosis-related inflammation.

IL-16 drives inflammation in ovarian endometriosis through CD4$^+$ T cells

Historically, IL-16 has been acknowledged as a chemoattractant for CD4$^+$ leukocytes, exerting its proinflammatory influence through interactions with CD4 and CD9, recognized as IL-16 receptors.[3,5] To scrutinize the role of IL-16 in recruiting specific proinflammatory cells within cystic fluid, we used 10× single-cell RNA sequencing (scRNA-seq) on sorted CD45$^+$ endometrial leukocytes from RNE and EE throughout the secretory phase of the menstrual cycle (Figure S4A). This yielded 5,737 and 5,521 single-cell transcriptome profiles for leukocytes from RNE and EE samples, respectively, which were clustered into 10 distinct cell

(F) Weight analysis of endometriosis lesions from WT mice with surgically induced endometriosis (n = 5) and *IL16*KO mice with surgically induced endometriosis (n = 6), using an unpaired t test.
(G) Pain threshold analysis of WT mice with surgically induced endometriosis (n = 5) and *IL16*KO mice with surgically induced endometriosis (n = 6), using an unpaired t test.
(H) ELISA data revealing the levels of IL-16 in the serum of WT mice (n = 4), WT mice with surgically induced endometriosis (n = 7), and *IL16*KO mice with surgically induced endometriosis (n = 8), using an unpaired t test.
Results in (F)–(H) were obtained from 2 independent experiments.

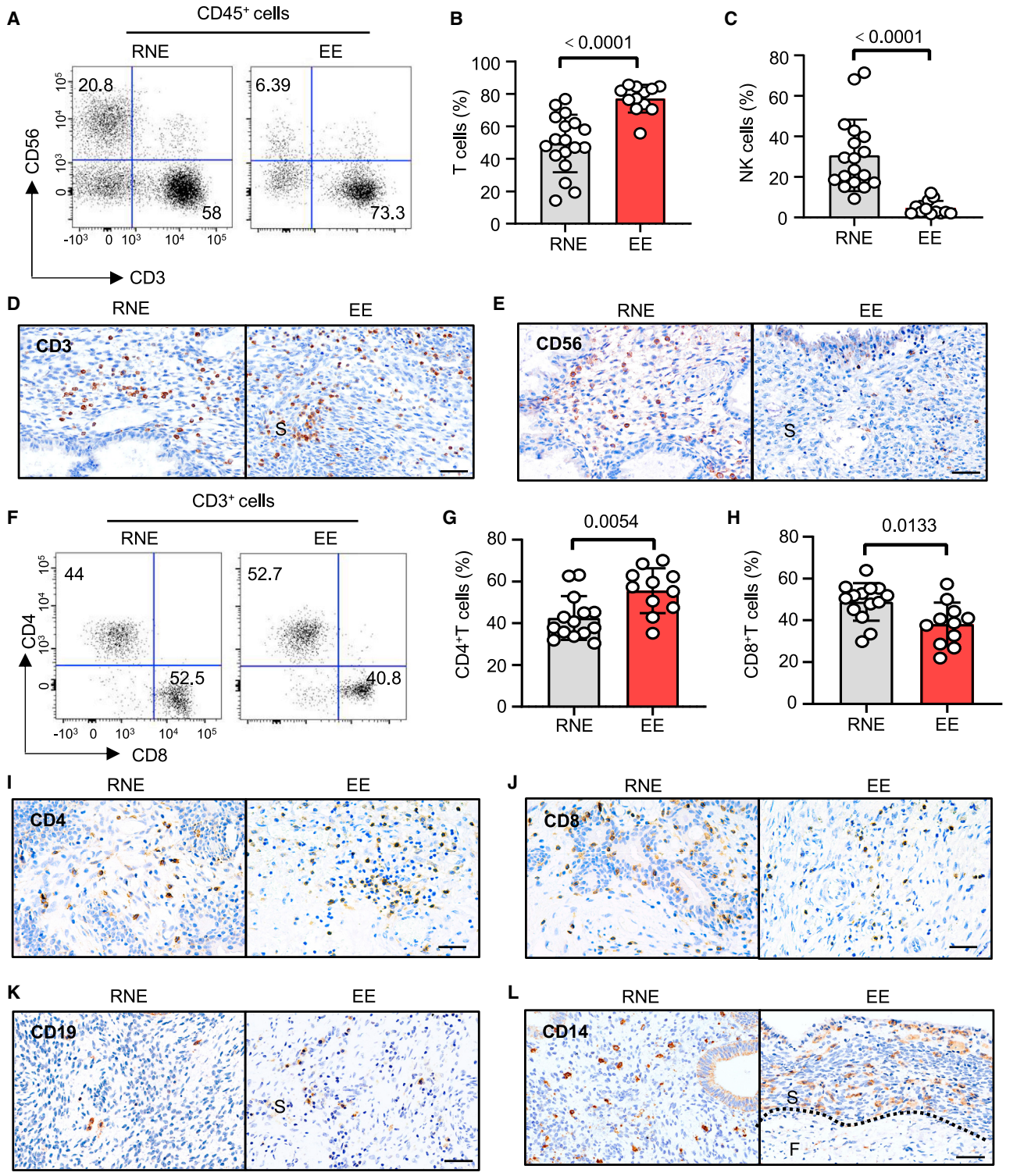

Figure 2. Increased infiltration of CD4⁺ T cells into the EE

(A) Representative analysis of CD3 and CD56 expression in CD45⁺ cells isolated from RNE or EE.

(B and C) Statistical analysis of the percentages of T cells ($CD3^+CD56^-$) (B) and NK cells ($CD3^-CD56^+$) (C) within the CD45⁺ cell population of the RNE (n = 18) or EE (n = 12), unpaired t test. Data represent a pool from multiple independent experiments.

(D and E) Representative micrographs of CD3 (D) and CD56 (E) IHC staining in RNE and EE cells; scale bar, 50 μm. Data are from at least 3 independent experiments.

(legend continued on next page)

clusters according to their expression signatures. T cells were identified as the predominant subtype in the EE (Figures S4B and S4C). Fluorescence-activated cell sorting (FACS) and IHC analyses further revealed augmented T cell infiltration and reduced NK cells in EE (Figures 2A–2E), particularly highlighting a significant increase in $CD4^+$ T cells (Figures 2F–2J). Single-cell sequencing also supported the augmentation of $CD4^+$ T cells in EE (Figure S4C). In addition, IHC results for B cells and macrophages in both RNE and EE were presented (Figures 2K and 2L). Collectively, these findings emphasize the role of IL-16 in facilitating $CD4^+$ T cell infiltration into EE.

Although prior research has demonstrated the ability of IL-16 to stimulate proinflammatory cytokines in PBMCs, its impact on endometriosis, specifically on $CD4^+$ T cells or other IL-16 receptor-positive cells, remained unexplored. Our study revealed a positive correlation between IL-16 in endometriosis patients' cystic fluid and the levels of IL-1β and IL-6 (Figures 3A and 3B). Furthermore, $CD4^+$ T cells from EE exhibited a higher capacity to produce IL-6 than $CD4^+$ T cells from RNE (Figures 3C and 3D). Building on these findings, we hypothesized that IL-16 may facilitate increased $CD4^+$ T cell infiltration into EE, promoting proinflammatory effects by enhancing IL-1β and IL-6 production within $CD4^+$ T cells.

To investigate the ability of IL-16 to induce the production of proinflammatory cytokines, including IL-6, in $CD4^+$ T cells, we cultured total PBMCs from healthy donors with active IL-16 at two concentrations (10 or 100 ng/mL). We assessed proinflammatory cytokine expression following 4 h of incubation. FACS analysis indicated a marked increase in IL-6 and TNF production within $CD4^+$ T cells treated with active IL-16 relative to the control group (Figures 3E–3H). Conversely, transforming growth factor β1 (TGF-β1) expression remained minimally affected (Figures 3I and 3J). Furthermore, the supernatant from total PBMCs cultured with active IL-16 was analyzed using a cytometric bead array (CBA), revealing significant upregulation of IL-6, IL-8, TNF, and IL-1β in the active IL-16-treated group compared to the control group (Figures 3K–3N). However, TGF-β1 expression remained relatively unaffected (Figure 3O).

Using single-cell sequencing data, we observed that endometriotic $CD4^+$ T cells exhibited an enhanced capacity to generate proinflammatory cytokines (Figure S5A). In addition, apoptotic and proinflammatory signaling pathways such as IL-17 and TNF were significantly elevated in ectopic endometrial $CD4^+$ T cells (Figure S5B). These results support the notion that inflammation in endometriosis is primarily promoted through $CD4^+$ T cells. Furthermore, our data suggested that the effect of IL-16 acted upstream of IL-6, because stimulation with IL-6 did not lead to an increase in active IL-16 in the culture supernatants of total PBMCs (Figure 3P). In summary, these findings provide compelling evidence that IL-16 is critical in initiating inflammation through $CD4^+$ T cells in endometriosis, emphasizing its potential as a therapeutic target for this condition.

Active IL-16 is primarily derived from ectopic endometrial T cells

Previous studies have underscored that IL-16 is predominantly expressed within immune cells.[40,41] Our IHC results unveiled both intra- and extracellular IL-16 in the EE, whereas only intracellular IL-16 was detected in the RNE. Intriguingly, IL-16 was primarily expressed in cells exhibiting a higher nuclear-to-cytoplasmic ratio, which, in line with our earlier findings, likely corresponds to T cells (Figure 4A). This observation suggests that IL-16 is secreted by cells within the EE. Moreover, a substantial level of IL-6 was observed in the EE (Figure 4B).

To ascertain whether T cells serve as the primary IL-16 source within ectopic endometrial tissue, we reevaluated the scRNA-seq data, revealing higher IL-16 expression in T cells relative to other cell types (Figure 4C). Supporting these findings, our confocal microscopy demonstrated IL-16 expression in $CD3^+$ T cells but not $CD163^+$ macrophages (Figure 4D). Although we did not observe an increase in IL-16 expression at the mRNA level in ectopic endometrial T cells (Figure 4E), active IL-16 protein (functional form) was detected through western blot (WB) analysis of sorted ectopic endometrial T cells (Figure 4F). Furthermore, a significant increase in IL-16 was noted in the supernatant of ectopic endometrial T cell cultures relative to relatively normal endometrial T cell cultures (Figure 4G). These findings suggest that T cells constitute the predominant immune cell subset in ectopic endometrial tissue and that the capacity of ectopic endometrial T cells to produce active IL-16 is significantly heightened compared to relatively normal endometrial T cells. Therefore, we propose that active IL-16 is primarily derived from ectopic endometrial T cells in ovarian endometriosis.

The activation of IL-16 in ectopic endometrial T cells is caused by iron overload

To explore the potential causes of active IL-16 release in ectopic endometrial T cells, we initially investigated environmental stress as a plausible factor. Our antibody array findings revealed elevated levels of ferritin and transferritin in the cystic fluid, ranking eighth and tenth among detected cytokines (Figure S2B). Ferritin, a marker for body iron storage indicating iron overload,[42,43] was further confirmed through Prussian blue staining, revealing increased iron content in the EE (Figure 5A). Similarly, the presence of Fe^{2+} and ferritin in the cystic fluid of patients with ovarian endometriosis was observed (Figures 5B and 5C). WB analysis quantified ferritin levels in ectopic endometrial tissue compared to relatively normal tissue (Figure 5D), confirming an iron-enriched microenvironment in the EE. Through scRNA-seq we observed a slight increase trend in *FTH1* (ferritin heavy chain 1) expression in ectopic endometrial T cells (Figure S5C). Consistent with this result, our qPCR and immunofluorescence data demonstrated upregulated FTH1 levels (Figures 5E and 5F).

(F) Representative analysis of CD4 and CD8 proportions in $CD45^+CD3^+CD56^-$ cells isolated from the RNE or EE.
(G and H) Statistical analysis of the percentages of CD4T cells ($CD4^+CD8^-$) (G) and CD8T cells ($CD8^+CD4^-$) (H) within the $CD45^+CD3^+CD56^-$ cell population, RNE (n = 14) and EE (n = 11), unpaired t test. Data represent a pool from multiple independent experiments.
(I–L) Representative micrographs of CD4 (I), CD8 (J), CD19 (K), and CD14 (L) IHC staining in RNE and EE cells; scale bar, 50 μm. Data are from at least 3 independent experiments.
All of the samples used for analysis in this figure were in the secretory phase.

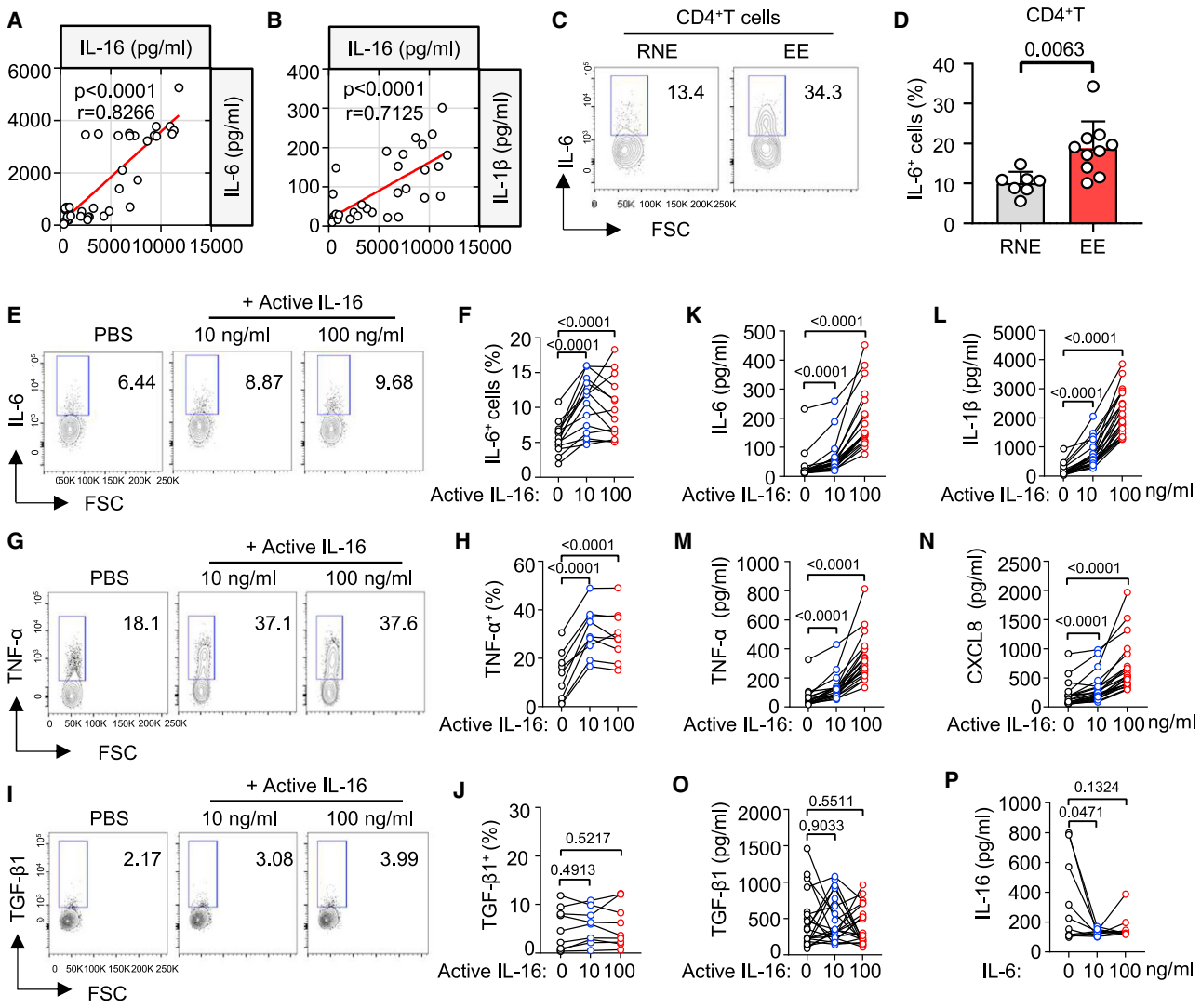

Figure 3. Active IL-16 promotes the production of IL-1β, IL-6, IL-8, and TNF

(A) Correlation analysis between IL-16 and IL-6 using the Spearman correlation method.

(B) Correlation analysis between IL-16 and IL-1β using the Spearman correlation method.

(C) Representative analysis of IL-6 expression by $CD45^+CD56^-CD3^+CD4^+$ T cells isolated from the RNE and EE.

(D) Statistical analysis of the percentages of IL-6-producing T cells among the $CD4^+$ T cell population isolated from the RNE (n = 9) and EE (n = 10), unpaired t test. Data represent a pool from multiple independent experiments.

(E, G, and I) PBMCs from a healthy donor were cultured with or without active IL-16 (10 or 100 ng/mL). For the detection of TNF, each group of cells was treated with phorbol myristate acetate (50 ng/mL), ionomycin (1 μg/mL), and monensin (10 μg/mL). After 4 h, the expression of IL-6, TNF, and TGF-β1 was determined by intracellular staining.

(F, H, and J) Statistical analysis of the percentages of $IL\text{-}6^+$, TNF^+, and $TGF\text{-}\beta1^+$ cells among the $CD4^+$ T cell population, paired t test, IL-6 (n = 14), TNF (n = 9), and TGF-β1 (n = 9).

Data in (E)–(J) represent a pool from multiple independent experiments.

(K–O) PBMCs from a healthy donor were stimulated for 12 h in the presence of PBS or different concentrations of active IL-16 (10 or 100 ng/mL), after which the production of IL-6, IL-1β, TNF, CXCL8, and TGF-β in cell supernatants was analyzed using a CBA assay, paired t test, n = 21.

(P) PBMCs from a healthy donor were stimulated for 12 h in the presence of PBS or different concentrations of IL-6 (10 or 100 ng/mL), after which the production of IL-16 in cell supernatants was analyzed using ELISA, paired t test, n = 10.

Data in (K)–(P) represent a pool from multiple independent experiments.

To further investigate elevated ferritin levels in ectopic endometrial T cells, we simulated the iron-rich microenvironment using Jurkat cells treated with cystic fluid. Notably, cystic fluid induced ferritin protein expression in Jurkat cells, an effect mitigated by deferoxamine (DFO), an iron chelator (Figures 5G and 5H). Concurrently, we observed heightened ferritin mRNA levels in Jurkat cells treated with iron dextran in a concentration-dependent manner (Figure 5I). These findings imply that iron within cystic fluid drives

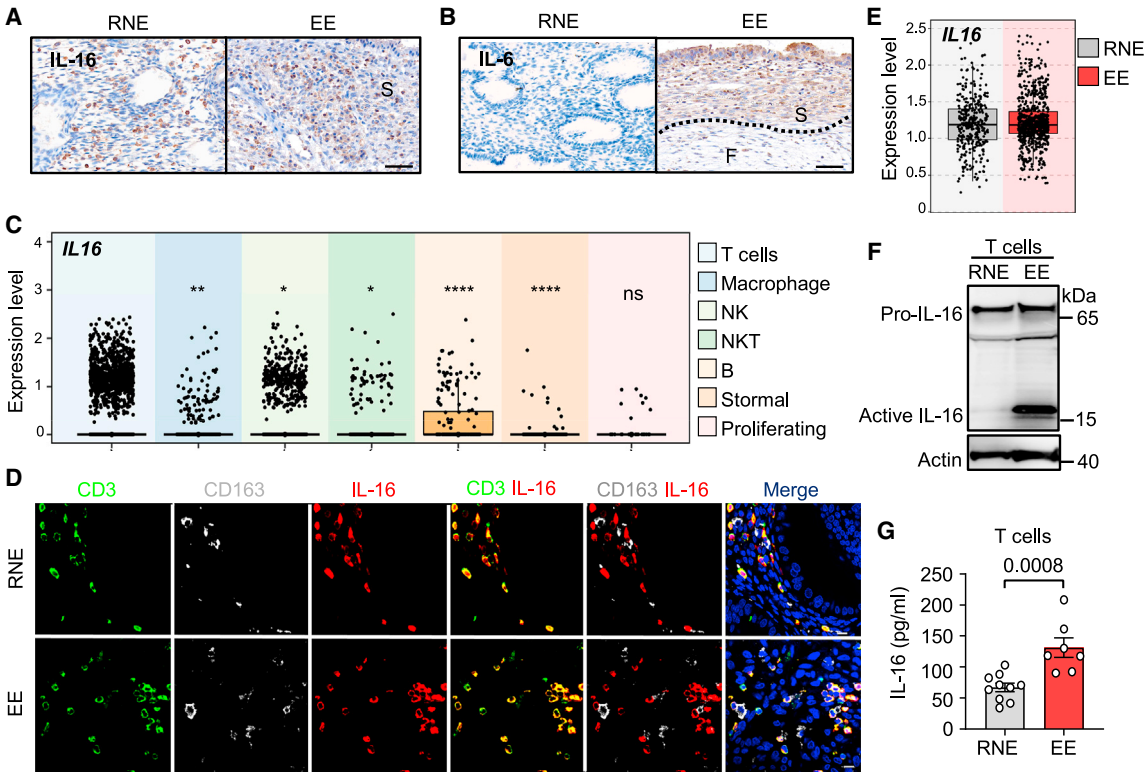

Figure 4. Active IL-16 in cystic fluid is released from ectopic endometrial T cells

(A and B) Representative micrographs of IL-16 (A) and IL-6 (B) IHC staining in RNE and EE. Scale bar, 50 μm. Data are from at least 3 independent experiments.

(C) The *IL16* expression levels in T cells (including CD4T, CD8T, and Foxp3$^+$T cells), macrophage, NK, NK T cells, B cells, stromal cells, and proliferating cells.

(D) Representative confocal micrographs of the expression of CD3, CD163, and IL-16 in RNE and EE. Scale bar, 10 μm. Data represents 2 independent experiments.

(E) The *IL16* expression level in RNE and EE cells (the T cells subsets including CD4T, CD8T, and Foxp3$^+$T cells).

(F) Immunoblotting of IL-16 in T cells from the RNE (n = 3) or EE (n = 4); antibodies against IL-16 recognized the full-length and C-terminal cleavage product. Data represent 2 independent experiments.

(G) The levels of IL-16 in cell culture supernatants from RNE and EE T cells were assessed by ELISA after 24 h (20,000 cells/well); RNE (n = 10); EE (n = 8); unpaired t test. Data represent a pool of multiple independent experiments.

heightened ferritin expression in T cells, potentially leading to iron accumulation and eventual overload.

Subsequently, we hypothesized that iron overload may drive IL-16 activation in ectopic endometrial T cells. To explore this, we exposed Jurkat cells to cystic fluid and confirmed its role in stimulating IL-16 activation (Figure 5J). DFO treatment inhibited IL-16 activation caused by cystic fluid exposure (Figure 5K). To confirm this hypothesis, we used iron dextran to directly activate IL-16 production in relatively normal endometrial T cells, a process impeded by DFO (Figures 5L-5M). These results suggest that iron overload triggers IL-16 activation in ectopic endometrial T cells.

A previous study illustrated that IL-16 activation relies upon active caspase-3-mediated processing.[2] Another study demonstrated that iron-activated reactive oxygen species can induce caspase-3-GSDME-mediated pyroptosis.[44] Our findings indicated that in comparison to relatively normal T cells, ectopic endometrial T cells displayed significantly lowered mitochondrial content and diminished mitochondrial membrane potential, indicating mitochondrial impairment (Figures S6A, S6B, S6C, and S6D, respectively). Treatment of Jurkat cells with iron dextran resulted in a decline in mitochondrial membrane potential, indicative of mitochondrial impairment (Figures S6E and S6F). FACS assays demonstrated higher levels of active caspase-3 in ectopic endometrial T cells compared to relatively normal T cells (Figures 5N and 5O). Furthermore, we observed the activation of caspase-3 and IL-16 in Jurkat cells upon iron dextran treatment (Figure 5P). Impressively, the introduction of the caspase-3 inhibitor Z-DEVD-FMK halted IL-16 release from ectopic endometrial T cells (Figure 5Q). Collectively, these findings underscore the role of an iron-enriched microenvironment in inducing iron overload within ectopic endometrial T cells, consequently driving caspase-3 and IL-16 activation.

The release of active IL-16 occurs through the caspase-3-GSDME-mediated pyroptosis pathway

After illuminating the mechanism of IL-16 activation, our focus transitioned to determining how T cells release active IL-16 into the extracellular environment. Structurally, IL-16 lacks a secretion signal, akin to other cytokines such as IL-1α, IL-1β, IL-33, and HMGB1, as reported by Rider et al..[41] The absence

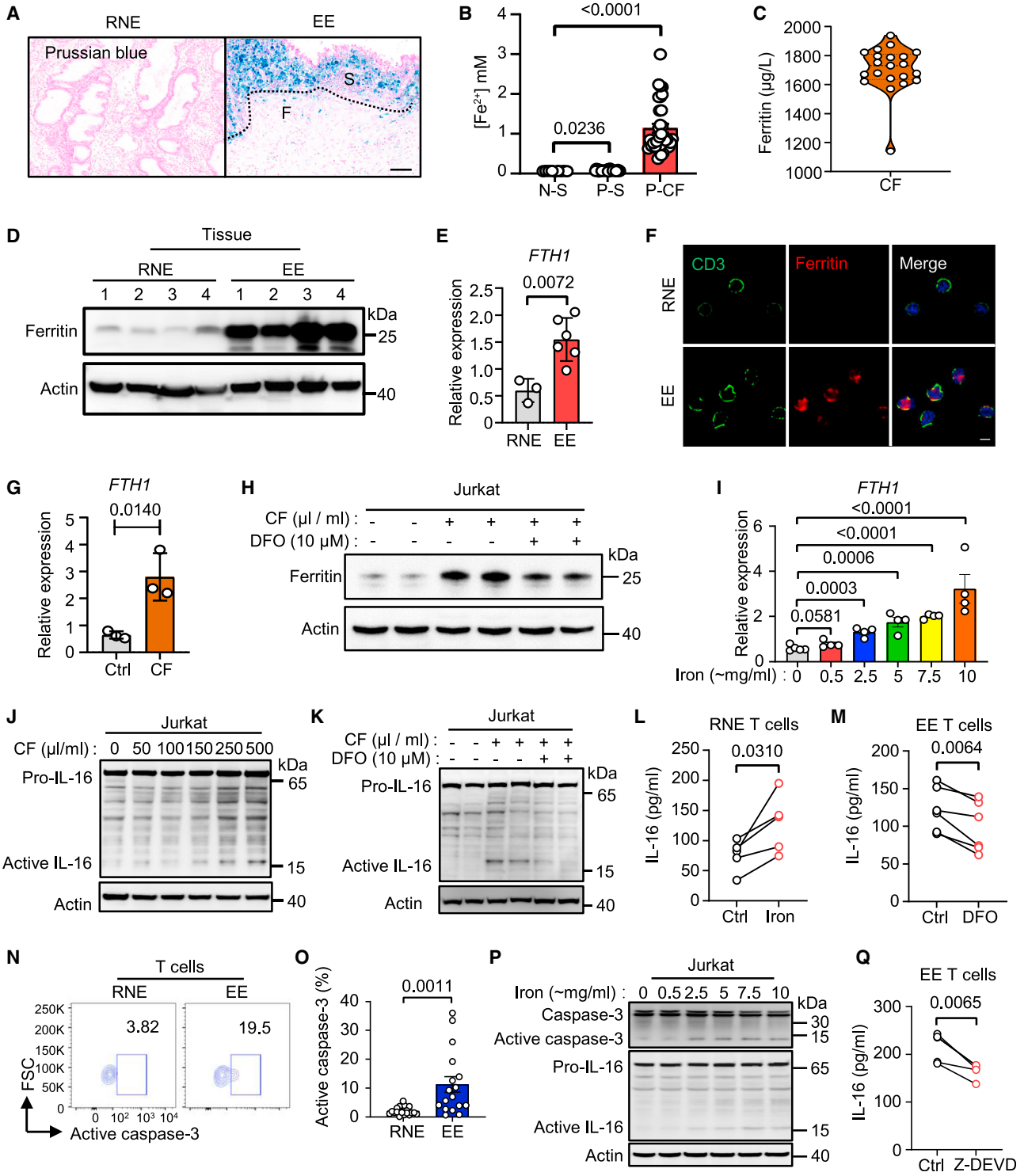

Figure 5. Cystic fluid causes iron enrichment in ectopic endometrial T cells and the release of active IL-16 in a caspase-3-dependent manner

(A) Representative image of Perls' Prussian blue staining of the RNE and EE; scale bar, 100 μm.

(B) Iron (Fe^{2+}) assay in normal human serum (N-S) (n = 9), endometriosis patient serum (P-S) (n = 31), and cystic fluid (P-CF) (n = 33).

(C) ELISA data illustrating the levels of ferritin in the cystic fluid (CF) (n = 21); serum ferritin concentrations are generally within the range of 15–300 μg/L.

(D) WB analysis of ferritin in RNE (n = 4) and EE tissues (n = 4).

(E) *FTH1* mRNA levels were examined by quantitative real-time PCR and normalized to *ACTB* expression.

(F) Confocal microscopic images of ferritin expression in T cells isolated from the RNE and EE; scale bar, 5 μm.

(legend continued on next page)

of a secretion signal prevents these cytokines from being released using a conventional secretory pathway. Several studies suggest that cytokines without secretion signals can be passively excreted from injured or necrotic cells, with pyroptosis and necroptosis implicated.[33,45,46] Although the mechanism for active IL-16 release remains unclear, prior studies indicate that active IL-16 release may be linked to cell death.[40,47,48]

Iron overload has been demonstrated to induce ferroptosis, a type of programmed cell death characterized by lipid peroxide accumulation. The downregulation of glutathione peroxidase 4 (GPX4) is a hallmark of ferroptosis.[49] Given that ectopic endometrial T cells exist in an iron-overloaded state, we examined whether ferroptosis plays a role in the release of active IL-16. Although we did not observe significant GPX4 upregulation in scRNA-seq (Figure S5C), qPCR and WB revealed noteworthy GPX4 upregulation in ectopic endometrial T cells (Figures 6A and 6B). Furthermore, ectopic endometrial T cells did not exhibit a significant increase in intracellular lipid peroxidation (Figures 6C and 6D). Treatment of Jurkat cells with cystic fluid and this concentration of iron dextran was insufficient to induce ferroptosis in Jurkat cells (Figures 6E and 6F). Taken together, our findings indicate that ferroptosis is not involved in releasing active IL-16.

Traditionally, caspase-3 has been classified as an executioner caspase due to its pivotal role in cell apoptosis. However, apoptosis is a nonlytic programmed cell death usually carried out without releasing harmful substances into the surrounding area.[50] Consequently, although IL-16 activation hinges on caspase-3, releasing active IL-16 is unlikely to be associated with caspase-3-mediated apoptosis. Recently, caspase-3 has been identified as a pyroptosis catalyst in tumor cells via GSDME cleavage.[51] These findings provide a potential reason for the release of active IL-16.

To explore the potential role of caspase-3-GSDME-mediated pyroptosis in the release of active IL-16 from T cells, we began by quantifying GSDME levels using IHC staining. Our observations revealed that total GSDME was elevated in ectopic endometrial tissues compared to relatively normal endometrial tissues (Figure 6G). Subsequently, we performed WB analysis on T cells acquired from relatively normal and ectopic endometrial tissues, alongside PBMCs, to assess pro-GSDME and the GSDME N-terminal domain (NTD) expression. Pro-GSDME and GSDME-NTD exhibited heightened expression in ectopic endometrial T cells compared to other sources (Figure 6H). Moreover, we transfected GSDME-NTD-mCherry into 293T cells expressing active IL-16-GFP to plot GFP and mCherry signal dynamics. Interestingly, our findings suggested a reduction in the IL-16-GFP signal upon GSDME-NTD-mCherry construct aggregation at the cell membrane, implying that GSDME-NTD-mediated pyroptosis triggered active IL-16 release (Figures 6I and 6J;Video S1).

To substantiate that iron overload indeed prompts GSDME$^+$ T cells to undergo pyroptosis, leading to active IL-16 release, we induced Jurkat cells into an iron-overloaded state through exposure to iron dextran. We identified morphological alterations aligned with pyroptosis on the cell membrane, characterized by swelling, pore formation, and rupture (Figure 6K). Subsequent examination revealed that levels of active caspase-3, GSDME-NTD, and active IL-16 were elevated with prolonged time (Figure 6L). These findings underscore that iron overload can initiate caspase-3-GSDME-mediated pyroptosis, resulting in the activation of IL-16 release.

Z30702029 inhibited the release of active IL-16

Building upon the earlier revelations, a compelling hypothesis emerged: could obstructing GSDME-mediated pyroptosis impede the liberation of active IL-16 by ectopic endometrial T cells? Recent structural analyses of gasdermin D (GSDMD) unveiled two aromatic residues, F50 and W51, in murine (m)GSDMD, and F49 and W50 in human (h)GSDMD, positioned at the center of the β1-β2 loop, conserved across gasdermin family members. Intriguingly, mutations targeting F50 and W51 in mGSDMD have been shown to significantly compromise the capacity of the NTD to initiate pyroptotic cell death.[52] A parallel scenario unfolds in hGSDME, where F43 and W44 occupy a comparable position to these pivotal amino acids.

In the quest for a viable compound to impede GSDME, we used Phyre2 to predict the crystal structure of hGSDME. The analysis uncovered a pocket formed by R42, F43, and W44 (Figure 7A). To scrutinize the involvement of the conserved sequence in the pore-forming role of GSDME NTD, we introduced glycine (G) substitutions for R42, F43, and W44 in hGSDME (Figure 7A).

(G) Jurkat cells were treated with cystic fluid (250 μL/mL) from a patient with endometriosis for 24 h, and *FTH1* mRNA levels were analyzed by quantitative real-time PCR and normalized to *ACTB* expression.
(H) Jurkat cells were treated with cystic fluid (250 μL/mL) from a patient with endometriosis for 24 h in a medium with or without DFO (10 μM).
(I) Quantitative real-time PCR analysis of Jurkat cells at 24 h in the presence of various concentrations of iron dextran (0, 0.5, 2.5, 50 7.5, or 10 mg/mL); *FTH1* mRNA levels were normalized to *ACTB* expression.
(J) Jurkat cells were treated with different concentrations (0, 50, 100, 150, 250, or 500 μL/mL) of cystic fluid from an endometriosis patient for 12 h. The expression of IL-16 was examined by immunoblotting.
(K) Jurkat cells were treated with cystic fluid (250 μL/mL) from a patient with endometriosis for 24 h in a medium with or without DFO (10 μM); IL-16 expression was assessed by immunoblotting.
(L) RNE T cells (n = 5) were cultured in a medium with or without iron dextran (5 μL/mL) for 24 h. The levels of active IL-16 in the cell culture supernatants were assessed by ELISA (n = 5; 20,000 cells/well).
(M) EE T cells (n = 6) were cultured in a medium with or without DFO (10 μM) for 24 h. The levels of active IL-16 in the cell culture supernatants were assessed by ELISA (n = 6; 20,000 cells/well).
(N) Analysis of active caspase-3 expression in $CD45^+CD3^+CD56^-$ cells isolated from the RNE or EE.
(O) Statistical assessment of the percentages of active caspase-3$^+$ cells in $CD45^+CD3^+CD56^-$ cells (unpaired t test); RNE, n = 19 and EE, n = 18.
(P) Immunoblotting analysis of caspase-3 and IL-16 in Jurkat cells at 24 h in the presence of various concentrations of iron dextran (0, 0.5, 2.5, 5, 7.5, or 10 mg/mL).
(Q) EE T cells (n = 5) cultured in a medium with or without Z-DEVD-FMK (50 μM) for 24 h. The levels of active IL-16 in cell culture supernatants were examined by ELISA (n = 5; 20,000 cells/well). Data are representative or are pooled from at least 2 independent experiments.

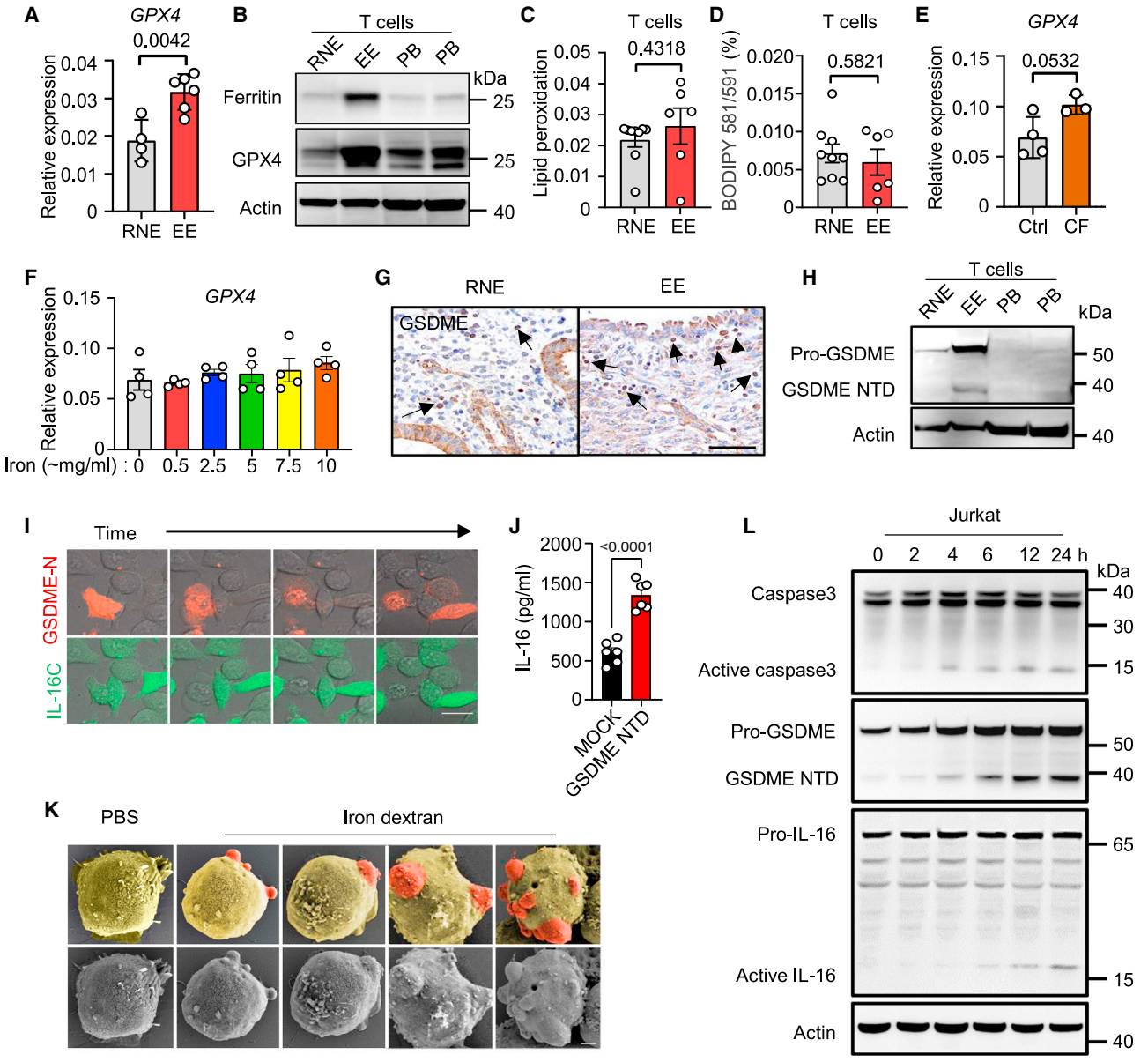

Figure 6. Ectopic endometrial T cells release active IL-16 via caspase-3-GSDME-mediated pyroptosis as opposed to ferroptosis

(A) *GPX4* mRNA levels in T cells from the RNE (n = 4) and EE (n = 6) analyzed by quantitative real-time PCR and normalized to *ACTB* expression.

(B) Immunoblotting of ferritin and GPX4 in RNE- (n = 7), EE- (n = 7), and PBMC-derived (n = 2) T cells.

(C) Quantification of the lipid peroxidation signal of T cells from the RNE (n = 9) and EE (n = 6).

(D) The lipid peroxidation of T cells in RNE (n = 9) and EE (n = 6); lipid peroxidation was examined using the BODIPY 581/591 C11 reagent, and the ratio between green fluorescence (oxidized) and red fluorescence (reduced) is displayed.

(E) Jurkat cells were treated with cystic fluid (250 μL/mL) from a patient with endometriosis for 24 h, and *GPX4* mRNA levels were analyzed by quantitative real-time PCR and normalized to *ACTB* expression.

(F) Quantitative real-time PCR analysis of Jurkat cells at 24 h in the presence of various concentrations of iron dextran (0, 0.5, 2.5, 5, 7.5, or 10 mg/mL). *FTH1* mRNA levels were normalized to *ACTB* expression.

(G) Representative image of IHC staining of GSDME in RNE and EE cells; scale bar, 50 μm.

(H) Immunoblotting of GSDME in T cells from the RNE (n = 7), EE (n = 7), and PBMCs (n = 2); anti-GSDME antibodies recognized the full and N-terminal cleavage products.

(I) Representative screenshots of the dynamic IL-16 release process. The complete videos for this experiment can be found in Video S1.

(J) Detection of active IL-16 in culture supernatant 24 h following transient transfection of MOCK or GSDME-NTD expressing plasmid in 293T cell lines with stable expression of active IL-16.

(legend continued on next page)

This alteration disrupted the pocket structure and significantly hampered lactate dehydrogenase (LDH) release (Figure 7B), establishing a causal link between the hGSDME pocket and GSDME-NTD-mediated pyroptosis. A subsequent virtual screening of the Enamine Advanced Library (50K) identified several compounds binding to the hGSDME NTD pocket (Figures 7C and S7A). The *in vitro* assessment of the cytotoxicity of Z30702029 in Jurkat cells, measured by LDH release, indicated minimal adverse effects (Figure 7D), Notably, Z30702029 effectively inhibited GSDME-NTD-mediated pyroptosis, evident from the reduced release of active IL-16 in iron-enriched conditions (Figure 7E). Expanding the investigation to primary ectopic endometrial T cells revealed that Z30702029 significantly curbed the release of active IL-16 (Figure 7F). These findings position Z30702029 as a promising candidate for blocking GSDME-NTD-mediated pyroptosis, holding potential therapeutic value in the context of endometriosis treatment.

Although the impact of Z30702029 on IL-16 release was initially observed *in vitro*, its influence on endometriosis development *in vivo* remained unexplored. To address this gap, we administered either Z30702029 or PBS to mice afflicted with endometriosis. Remarkably, the Z30702029-treated group exhibited significantly reduced ectopic lesion weights compared to the control group (Figures 7G and 7H). Consistently, the Z30702029-treated group displayed diminished pain symptoms and IL-16 levels (Figures 7I and 7J), aligned with our previous findings. Despite observing no significant alterations in proliferating cell nuclear antigen expression in the EE between the treated and untreated groups, a discernible reduction in IL-6 was evident in the Z30702029-treated ectopic endometrial tissue (Figures S7B and S7C). Collectively, these findings suggest that Z30702029 has the potential to inhibit GSDME-mediated pyroptosis, thereby suppressing the production of proinflammatory cytokines, leading to the attenuation of active IL-16 release and a subsequent reduction in endometriosis development.

DISCUSSION

This study sheds light on a crucial connection between iron overload-triggered GSDME-mediated pyroptosis and the release of active IL-16. Our results reveal that the iron-enriched microenvironment in ectopic endometrial T cells can activate caspase-3 and, consequently, GSDME-mediated pyroptosis. The implications of our findings extend beyond endometriosis alone. The evolving comprehension of GSDME-mediated pyroptosis as a mechanism for releasing active proinflammatory cytokines transcends the confines of this particular disease.

Our findings underscore the involvement of GSDME-mediated pyroptosis in releasing active IL-16, with broader implications for understanding the pathogenesis of various inflammatory disorders. These disorders include ovarian and breast cancer, melanoma, asthma, rheumatoid arthritis, and cardiovascular diseases.[17,53–57] The interplay among iron overload, GSDME-mediated pyroptosis, and active IL-16 release, as elucidated in our study, holds the potential to unveil similar underlying mechanisms in other inflammatory conditions.

Moreover, the discovery of Z30702029 as an inhibitor of GSDME-NTD-mediated pyroptosis not only provides a potential avenue for treating endometriosis but also introduces a therapeutic strategy for addressing inflammatory diseases associated with active IL-16 release. Focusing on the molecular mechanisms of pyroptosis, our results may lay the foundation for innovative approaches to regulating inflammatory responses, offering a comprehensive framework for therapeutic interventions in diverse inflammatory pathologies.

The intricate and multifaceted nature of endometriosis pathogenesis has been emphasized in previous studies, highlighting the central role of inflammation in propelling its advancement.[17,58,59] In a departure from earlier inquiries that predominantly focused on the peritoneal fluid in individuals with endometriosis,[60] our investigation provides fresh perspectives into the localized inflammatory responses within the EE, carrying substantial implications for the underlying mechanisms of the disease.

Recent findings have underscored the roles of T cell effector functions and macrophage-driven proinflammatory cytokine secretion in the escalation of endometriosis.[60,61] Although previous research, as exemplified by Tan et al., has initiated the characterization of the ectopic endometrial microenvironment, the intricate mechanisms through which inflammation propels endometriosis largely remain elusive.[62] Our study addresses this knowledge gap by revealing the pivotal role of T cells and active IL-16 in coordinating local inflammation within the ectopic endometrial microenvironment. The identification of excessive active IL-16 release by ectopic endometrial T cells, subsequently prompting the generation of proinflammatory cytokines in $CD4^+$ T cells, positions $CD4^+$ T cells as the primary immune cell subset steering local inflammation within the EE. Consequently, these insights carry implications for understanding endometriosis development and progression. Delving deeper into the roles of $CD4^+$ T cells and other immune subsets in endometriosis pathogenesis may pave the way for innovative therapeutic strategies to address this debilitating disorder.

In clinical practice, surgical resection and hormonal therapy stand as the primary curative treatments for endometriosis patients.[17,63] However, the recurrence rate of endometriosis postsurgery is approximately 21.5% at 2 years and exceeds 50% at 5 years.[64] Moreover, many treatment modalities come with undesirable side effects. Consequently, developing patient-centric therapies to alleviate endometriosis-associated symptoms has become a research priority. Given the hormonal dependency of endometriosis,[13,58,65] targeting hormone pathways has emerged as a treatment strategy. However, hormone therapies, such as estrogen suppression, bring significant side effects.[17,63,66] Therefore, identifying nonhormone

(K) Representative scanning electron microscopy micrographs of Jurkat cells incubated with iron dextran (25 μL/mL) or PBS for 24 h; scale bar, 1 μm. The upper row depicts the pseudocolored images, and the lower row illustrates the original images.
(L) Immunoblotting analysis of caspase-3, GSDME, and IL-16 in Jurkat cells at 7.5 mg/mL iron dextran in different time points (0, 2, 4, 6, 12, and 24 h). Data are representative or are pooled from at least 2 independent experiments.

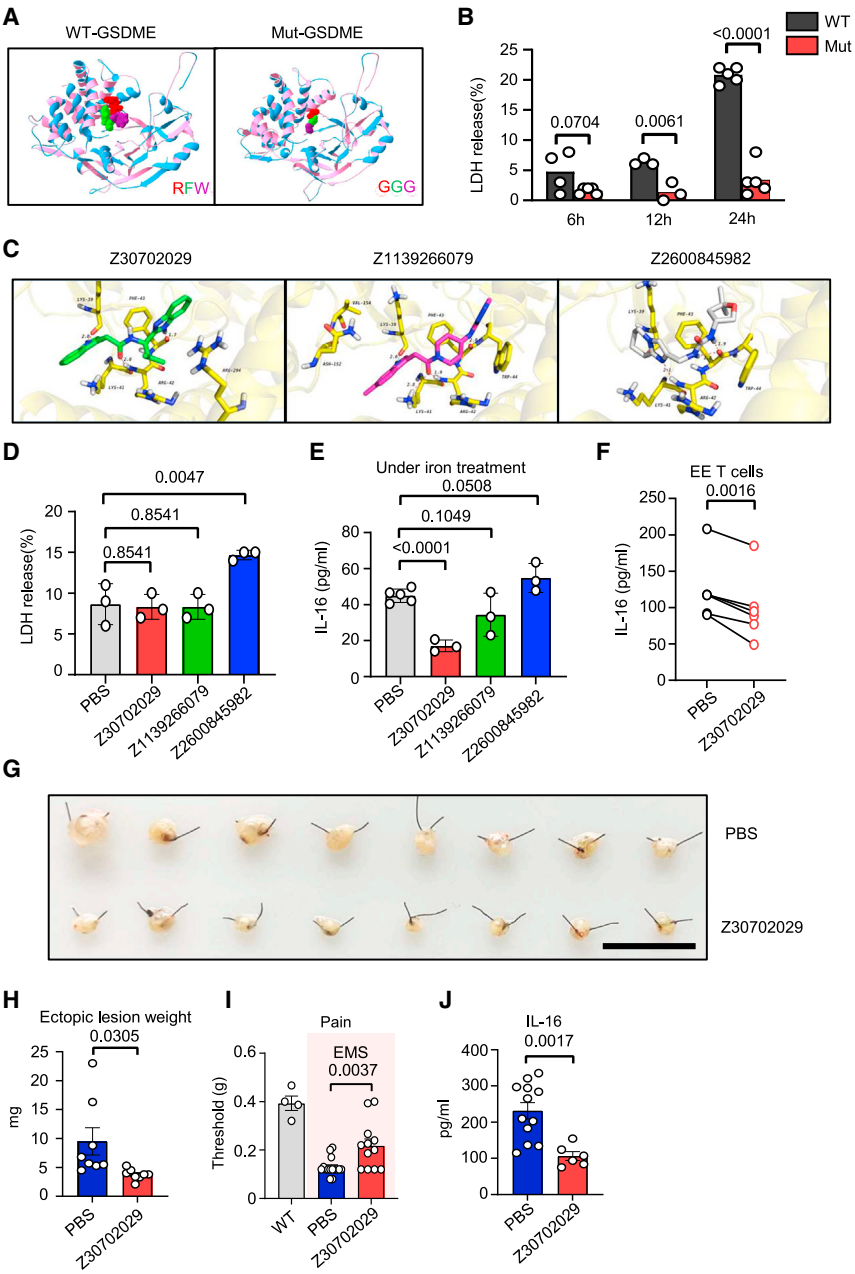

Figure 7. Inhibiting the function of the GSDME NTD can block the release of active IL-16

(A) Model of hGSDME predicted using the Phyre2 server based on the structure of hGSDMEA3. (Left) WT hGSDME model, with the 3 critical amino acids, 42R, 43F, and 44W, indicated in red, green, and purple, respectively. (Right) Mutant hGSDME model, and the alterations in the 3 critical amino acids, 42G, 43G, and 44G, are shown in red, green, and purple, respectively.

(B) The comparison of LDH release by 293T cells transfected with a plasmid containing the WT or mutant GSDME NTD at different time points (6, 12, or 24 h).

(C) A closeup view of the binding positions of the Z30702029, Z1139266079, and Z2600845982 compounds and the resulting GSDME pocket interfaces.

(D) Assessment of LDH levels in the cell culture supernatant after Jurkat cells cultured for 12 h in the presence of PBS or the compounds Z30702029, Z1139266079, or Z2600845982.

(E) ELISA analysis of IL-16 level in the supernatants of Jurkat cells after 12 h of incubation with iron dextran (2.5 mg/mL) alongside PBS or the compounds Z30702029, Z1139266079, or Z26008 45982 (each at 10 μM concentration).

(F) EE (n = 6) T cells were cultured in a medium with or without Z30702029 (10 μM) for 24 h. The levels of IL-16 in cell culture supernatants were examined by ELISA (n = 6; 20,000 cells/well).

(G) Ectopic lesions were isolated from WT mice with endometriosis intraperitoneally treated with PBS or Z30702029 (15 mg/kg), scale bar, 1 cm.

(H) Weight analysis of ectopic lesions isolated from C57BL/6J mice with endometriosis intraperitoneally treated with PBS (n = 8) or Z30702029 (n = 8), using an unpaired t test.

(I) Pain threshold analysis of WT mice and WT mice with endometriosis surgery intraperitoneally treated with PBS or Z30702029, using an unpaired t test.

(J) ELISA of IL-16 levels in the serum of WT mice with endometriosis intraperitoneally treated with PBS (n = 12) or Z30702029 (n = 6), using an unpaired t test. Data are representative or are pooled from at least 2 independent experiments.

therapeutic avenues is crucial. Inflammation is intricately linked to endometriosis-associated symptoms, highlighting the potential of targeting inflammation pathways as a promising approach.[67–71] Our study elucidates mechanisms underpinning endometriosis development and progression, particularly emphasizing the iron overload-caspase-3-GSDME-active IL-16 pathway. This pathway represents a promising direction for future therapeutic interventions. Our development of the compound Z30702029, disrupting GSDME NTD pore-formation capacity and inhibiting active IL-16 release, provides a potential avenue to modulate this pathway. Although its promising *in vitro* and murine model effects are encouraging, further assessment is warranted to gauge its therapeutic effectiveness.

In summary, our investigation not only enhances our comprehension of endometriosis pathogenesis but also expands the relevance of GSDME-mediated pyroptosis in instigating active cytokine release. This fresh perspective highlights the wider significance of our findings in unraveling the mechanisms propelling inflammation in diverse pathological contexts, thus unveiling another prospect for therapeutic interventions beyond endometriosis.

Limitations of the study

Several limitations must be considered when interpreting the outcomes of this study. First, it is essential to recognize that endometriosis encompasses various subtypes, including peritoneal

endometriosis, deep infiltrating endometriosis, and extrapelvic endometriosis, among others. Our investigation predominantly centered on ovarian endometriosis. Whether the mechanisms unveiled in this study possess universal applicability across different endometriosis subtypes requires further exploration. Second, the effectiveness of Z30702029 was primarily assessed *in vitro* and in mouse endometriosis models. Although these experimental setups yielded valuable insights, investigating the same therapeutic effects in larger animals, such as primates with spontaneously occurring endometriosis, demands further scrutiny. In addition, our study lacks a comprehensive exploration of the *in vivo* side effects of this compound. More extensive pharmacological and toxicological experiments must be conducted at preclinical stages using animal models that closely mimic human physiology.

STAR★METHODS

Detailed methods are provided in the online version of this paper and include the following:

- KEY RESOURCES TABLE
- RESOURCE AVAILABILITY
  - Lead contact
  - Materials availability
  - Data and code availability
- EXPERIMENTAL MODEL AND STUDY PARTICIPANT DETAILS
  - Human subjects
  - Mice
  - Human sample isolation
  - Surgically induced endometriosis
- METHOD DETAILS
  - The Von Frey filament test
  - Quantitative PCR analysis of ferritin heavy chain (FTH)1 and GPX4 expression
  - Histological analyses
  - Immunohistochemistry (IHC)
  - Multiplex immunohistochemistry (mIHC)
  - Immunofluorescence
  - Scanning electron microscopy (SEM)
  - Antibody array
  - Flow cytometry
  - Cell sorting using flow cytometry (flow sorting)
  - The enzyme-linked immunosorbent assay (ELISA)
  - Cytometric bead array (CBA) assay
  - Western blot analysis
  - Droplet-based scRNA-seq (10x chromium)
  - 10x scRNA-seq data processing
  - Data integration and cell type annotation
  - Lactate dehydrogenase (LDH) assay
  - Lipid peroxidation assay
  - Iron detection assay
- QUANTIFICATION AND STATISTICAL ANALYSIS

SUPPLEMENTAL INFORMATION

Supplemental information can be found online at https://doi.org/10.1016/j.xcrm.2024.101476.

ACKNOWLEDGMENTS

We thank all of the women who participated in our research. We are most grateful to Ms. Laihua Hu and Ms. Meiling Zhu for their help in collecting the samples for this study. This research was supported by the National Natural Science Foundation of China (U19A2024 and 81922028, to H.W.; 82201943 and WK9100000043, to J.Z.; and 32170932, to Y.Z.), the National Key Research & Developmental Program of China (2018YFC1003900 to H.W.), the Global Select Project of the Institute of Health and Medicine (PJK-Lx−2022004, to B.F.), and the National Key R&D Program of China (2022YFC2704003, to W.Z).

AUTHOR CONTRIBUTIONS

Conceptualization, H.W., B.F., and W.Z.; methodology, J.Z., S.X., X.X., and X.D.; formal analysis, J.Z. and X.Z.; investigation, H.W., B.F., and J.Z.; resources, W.Z., W.H., R.S., and Z.T.; data curation, B.F., J.Z., and X.Z.; writing – original draft, J.Z.; writing – review & editing, B.F. and H.W.; visualization, J.Z.; supervision, H.W.; project administration, B.F.; funding acquisition, H.W., B.F., J.Z., and Y.Z.

DECLARATION OF INTERESTS

The authors declare no competing interests.

Received: November 7, 2022
Revised: January 9, 2024
Accepted: February 21, 2024
Published: March 19, 2024

REFERENCES

1. Center, W.C.a.D.M. (1982). Modulation of lymphocyte migration by human lymphokines. II. Purification of a lymphotactic factor (LCF). The journal of immunology *128*.
2. Zhang, Y., Center, D.M., Wu, D.M., Cruikshank, W.W., Yuan, J., Andrews, D.W., and Kornfeld, H. (1998). Processing and activation of pro-interleukin-16 by caspase-3. J. Biol. Chem. *273*, 1144–1149. https://doi.org/10.1074/jbc.273.2.1144.
3. Liu, Y., Cruikshank, W.W., O'Loughlin, T., O'Reilly, P., Center, D.M., and Kornfeld, H. (1999). Identification of a CD4 domain required for interleukin-16 binding and lymphocyte activation. J. Biol. Chem. *274*, 23387–23395. https://doi.org/10.1074/jbc.274.33.23387.
4. Nicoll, J., Cruikshank, W.W., Brazer, W., Liu, Y., Center, D.M., and Kornfeld, H. (1999). Identification of domains in IL-16 critical for biological activity. J. Immunol. *163*, 1827–1832.
5. Qi JC, W.J., Mandadi, S., Tanaka, K., Roufogalis, B.D., Madigan, M.C., Lai, K., Yan, F., Chong, B.H., Stevens, R.L., and Krilis, S.A. (2006). Human and mouse mast cells use the tetraspanin CD9 as an alternate interleukin-16 receptor. Blood *107*, 135–142. https://doi.org/10.1182/blood-2005-03-factors.
6. Mathy, N.L., Scheuer, W., Lanzendörfer, M., Ambrosius, D., Norley, S., Kurth, R., and Honold, K. (2000). Interleukin-16 stimulates the expression and production of pro-inflammatory cytokines by human monocytes. Immunology *100*, 63–69.
7. Zhang, J., Yang, Z., Liang, Z., Wang, M., Hu, C., Chang, C., Shi, L., Ji, Q., and Liu, L. (2021). Anti-Interleukin-16 Neutralizing Antibody Treatment Alleviates Sepsis-Induced Cardiac Injury and Dysfunction via the Nuclear Factor Erythroid-2 Related Factor 2 Pathway in Mice. Oxid. Med. Cell. Longev. *2021*, 6616422. https://doi.org/10.1155/2021/6616422.
8. Kawabata, K., Makino, T., Makino, K., Kajihara, I., Fukushima, S., and Ihn, H. (2020). IL-16 expression is increased in the skin and sera of patients with systemic sclerosis. Rheumatology *59*, 519–523. https://doi.org/10.1093/rheumatology/kez318.

9. Qin, X.J., Shi, H.Z., Huang, Z.X., Kang, L.F., Mo, W.N., and Wu, C. (2005). Interleukin-16 in tuberculous and malignant pleural effusions. Eur. Respir. J. *25*, 605–611. https://doi.org/10.1183/09031936.05.00090804.

10. Blaschke, S., Schulz, H., Schwarz, G., Müller, G.A., Müller, G.A., and Reuss-Borst, M. (2001). Interleukin 16 expression in relation to disease activity in rheumatoid arthritis. J. Rheumatol. *28*, 12–21.

11. Seegert, D., Rosenstiel, P., Pfahler, H., Pfefferkorn, P., Nikolaus, S., and Schreiber, S. (2001). Increased expression of IL-16 in inflammatory bowel disease. Gut *48*, 326–332.

12. Skundric, D.S., Cruikshank, W.W., and Drulovic, J. (2015). Role of IL-16 in CD4+ T cell-mediated regulation of relapsing multiple sclerosis. J. Neuroinflammation *12*, 78. https://doi.org/10.1186/s12974-015-0292-x.

13. Zondervan, K.T., Becker, C.M., and Missmer, S.A. (2020). Endometriosis. N. Engl. J. Med. *382*, 1244–1256. https://doi.org/10.1056/NEJMra1810764.

14. Broi, M.G.D., Ferriani, R.A., and Navarro, P.A. (2019). Ethiopathogenic mechanisms of endometriosis-related infertility. JBRA Assist. Reprod. *23*, 273–280. https://doi.org/10.5935/1518-0557.20190029.

15. Meuleman, C., Vandenabeele, B., Fieuws, S., Spiessens, C., Timmerman, D., and D'Hooghe, T. (2009). High prevalence of endometriosis in infertile women with normal ovulation and normospermic partners. Fertil. Steril. *92*, 68–74. https://doi.org/10.1016/j.fertnstert.2008.04.056.

16. Tomassetti, C., and D'Hooghe, T. (2018). Endometriosis and infertility: Insights into the causal link and management strategies. Best Pract. Res. Clin. Obstet. Gynaecol. *51*, 25–33. https://doi.org/10.1016/j.bpobgyn.2018.06.002.

17. Saunders, P.T.K., and Horne, A.W. (2021). Endometriosis: Etiology, pathobiology, and therapeutic prospects. Cell *184*, 2807–2824. https://doi.org/10.1016/j.cell.2021.04.041.

18. Della Corte, L., Di Filippo, C., Gabrielli, O., Reppuccia, S., La Rosa, V.L., Ragusa, R., Fichera, M., Commodari, E., Bifulco, G., and Giampaolino, P. (2020). The Burden of Endometriosis on Women's Lifespan: A Narrative Overview on Quality of Life and Psychosocial Wellbeing. Int. J. Environ. Res. Public Health *17*, 4683. https://doi.org/10.3390/ijerph17134683.

19. Horne, A.W., and Saunders, P.T.K. (2019). SnapShot: Endometriosis. Cell *179*, 1677–1677.e1. https://doi.org/10.1016/j.cell.2019.11.033.

20. Riccio, L.d.G.C., Santulli, P., Marcellin, L., Abrão, M.S., Batteux, F., and Chapron, C. (2018). Immunology of endometriosis. Best Pract. Res. Clin. Obstet. Gynaecol. *50*, 39–49. https://doi.org/10.1016/j.bpobgyn.2018.01.010.

21. Berkley, K.J., Rapkin, A.J., and Papka, R.E. (2005). The pains of endometriosis. Science *308*, 1587–1589. https://doi.org/10.1126/science.1111445.

22. Dominique, B.B., and Chapron, C. (2010). Endometriosis and infertility: pathophysiology and management. Lancet *376*.

23. Evans, S., Moalem-Taylor, G., and Tracey, D.J. (2007). Pain and endometriosis. Pain *132*, S22–S25. https://doi.org/10.1016/j.pain.2007.07.006.

24. Mohammed Rasheed, H.A., and Hamid, P. (2020). Inflammation to Infertility: Panoramic View on Endometriosis. Cureus *12*, e11516. https://doi.org/10.7759/cureus.11516.

25. Maddern, J., Grundy, L., Castro, J., and Brierley, S.M. (2020). Pain in Endometriosis. Front. Cell. Neurosci. *14*, 590823. https://doi.org/10.3389/fncel.2020.590823.

26. Morotti, M., Vincent, K., and Becker, C.M. (2017). Mechanisms of pain in endometriosis. Eur. J. Obstet. Gynecol. Reprod. Biol. *209*, 8–13. https://doi.org/10.1016/j.ejogrb.2016.07.497.

27. Forster, R., Sarginson, A., Velichkova, A., Hogg, C., Dorning, A., Horne, A.W., Saunders, P.T.K., and Greaves, E. (2019). Macrophage-derived insulin-like growth factor-1 is a key neurotrophic and nerve-sensitizing factor in pain associated with endometriosis. FASEB J *33*, 11210–11222. https://doi.org/10.1096/fj.201900797R.

28. Kato, T., Yasuda, K., Matsushita, K., Ishii, K.J., Hirota, S., Yoshimoto, T., and Shibahara, H. (2019). Interleukin-1/-33 Signaling Pathways as Therapeutic Targets for Endometriosis. Front. Immunol. *10*, 2021. https://doi.org/10.3389/fimmu.2019.02021.

29. Ahn, S.H., Khalaj, K., Young, S.L., Lessey, B.A., Koti, M., and Tayade, C. (2016). Immune-inflammation gene signatures in endometriosis patients. Fertil. Steril. *106*, 1420–1431.e7. https://doi.org/10.1016/j.fertnstert.2016.07.005.

30. Bersinger, N.A., von Roten, S., Wunder, D.M., Raio, L., Dreher, E., and Mueller, M.D. (2006). PAPP-A and osteoprotegerin, together with interleukin-8 and RANTES, are elevated in the peritoneal fluid of women with endometriosis. Am. J. Obstet. Gynecol. *195*, 103–108. https://doi.org/10.1016/j.ajog.2005.12.010.

31. Kyama, S.D., Mwenda, J.M., and Thomas, M D'Hooghe (2003). Potential involvement of the immune system in the development of endometriosis. Reprod Biol Endocrino *1*.

32. Lin, Y.H., Chen, Y.H., Chang, H.Y., Au, H.K., Tzeng, C.R., and Huang, Y.H. (2018). Chronic Niche Inflammation in Endometriosis-Associated Infertility: Current Understanding and Future Therapeutic Strategies. Int. J. Mol. Sci. *19*, 2385. https://doi.org/10.3390/ijms19082385.

33. Evavold, C.L., Ruan, J., Tan, Y., Xia, S., Wu, H., and Kagan, J.C. (2018). The Pore-Forming Protein Gasdermin D Regulates Interleukin-1 Secretion from Living Macrophages. Immunity *48*, 35–44.e6. https://doi.org/10.1016/j.immuni.2017.11.013.

34. Sanchez, A.M., Viganò, P., Somigliana, E., Panina-Bordignon, P., Vercellini, P., and Candiani, M. (2014). The distinguishing cellular and molecular features of the endometriotic ovarian cyst: from pathophysiology to the potential endometrioma-mediated damage to the ovary. Hum. Reprod. Update *20*, 217–230. https://doi.org/10.1093/humupd/dmt053.

35. Tapmeier, T.T., Rahmioglu, N., Lin, J., De Leo, B., Obendorf, M., Raveendran, M., Fischer, O.M., Bafligil, C., Guo, M., Harris, R.A., et al. (2021). Neuropeptide S receptor 1 is a nonhormonal treatment target in endometriosis. Sci. Transl. Med. *13*, eabd6469. https://doi.org/10.1126/scitranslmed.abd6469.

36. Moalem, G., and Tracey, D.J. (2006). Immune and inflammatory mechanisms in neuropathic pain. Brain Res. Rev. *51*, 240–264. https://doi.org/10.1016/j.brainresrev.2005.11.004.

37. Koga, K., Osuga, Y., Yoshino, O., Hirota, Y., Yano, T., Tsutsumi, O., and Taketani, Y. (2005). Elevated interleukin-16 levels in the peritoneal fluid of women with endometriosis may be a mechanism for inflammatory reactions associated with endometriosis. Fertil. Steril. *83*, 878–882. https://doi.org/10.1016/j.fertnstert.2004.12.004.

38. Azimzadeh, P., Khorram Khorshid, H.R., Akhondi, M.M., and Shirazi, A. (2016). Association of interleukin-16 polymorphisms with disease progression and susceptibility in endometriosis. Int. J. Immunogenet. *43*, 297–302. https://doi.org/10.1111/iji.12281.

39. Matalliotakis, M., Zervou, M.I., Eliopoulos, E., Matalliotaki, C., Rahmioglu, N., Kalogiannidis, I., Zondervan, K., Spandidos, D.A., Matalliotakis, I., and Goulielmos, G.N. (2018). The role of IL16 gene polymorphisms in endometriosis. Int. J. Mol. Med. *41*, 1469–1476. https://doi.org/10.3892/ijmm.2018.3368.

40. Cruikshank, W.W., Kornfeld, H., and Center, D.M. (2000). Interleukin-16. J. Leukoc. Biol. *67*, 757–766.

41. Rider, P., Voronov, E., Dinarello, C.A., Apte, R.N., and Cohen, I. (2017). Alarmins: Feel the Stress. J. Immunol. *198*, 1395–1402. https://doi.org/10.4049/jimmunol.1601342.

42. Kang, H., Han, M., Xue, J., Baek, Y., Chang, J., Hu, S., Nam, H., Jo, M.J., El Fakhri, G., Hutchens, M.P., et al. (2019). Renal clearable nanochelators for iron overload therapy. Nat. Commun. *10*, 5134. https://doi.org/10.1038/s41467-019-13143-z.

43. Wang, X., Mendelsohn, L., Rogers, H., Leitman, S., Raghavachari, N., Yang, Y., Yau, Y.Y., Tallack, M., Perkins, A., Taylor, J.G., 6th., et al. (2014). Heme-bound iron activates placenta growth factor in erythroid cells via erythroid Kruppel-like factor. Blood *124*, 946–954. https://doi.org/10.1182/blood-2013-11-539718.

44. Zhou, B., Zhang, J.Y., Liu, X.S., Chen, H.Z., Ai, Y.L., Cheng, K., Sun, R.Y., Zhou, D., Han, J., and Wu, Q. (2018). Tom20 senses iron-activated ROS signaling to promote melanoma cell pyroptosis. Cell Res. *28*, 1171–1185. https://doi.org/10.1038/s41422-018-0090-y.

45. Monteleone, M., Stow, J.L., and Schroder, K. (2015). Mechanisms of unconventional secretion of IL-1 family cytokines. Cytokine *74*, 213–218. https://doi.org/10.1016/j.cyto.2015.03.022.

46. Scaffidi, P., Misteli, T., and Bianchi, M.E. (2002). Release of chromatin protein HMGB1 by necrotic cells triggers inflammation. Nature *418*, 191–195.

47. Elssner, A., Doseff, A.I., Duncan, M., Kotur, M., and Wewers, M.D. (2004). IL-16 is constitutively present in peripheral blood monocytes and spontaneously released during apoptosis. J. Immunol. *172*, 7721–7725. https://doi.org/10.4049/jimmunol.172.12.7721.

48. Roth, S., Solbach, W., and Laskay, T. (2016). IL-16 and MIF: messengers beyond neutrophil cell death. Cell Death Dis. *7*, e2049. https://doi.org/10.1038/cddis.2015.388.

49. Dixon, S.J., Lemberg, K.M., Lamprecht, M.R., Skouta, R., Zaitsev, E.M., Gleason, C.E., Patel, D.N., Bauer, A.J., Cantley, A.M., Yang, W.S., et al. (2012). Ferroptosis: an iron-dependent form of nonapoptotic cell death. Cell *149*, 1060–1072. https://doi.org/10.1016/j.cell.2012.03.042.

50. Bedoui, S., Herold, M.J., and Strasser, A. (2020). Emerging connectivity of programmed cell death pathways and its physiological implications. Nat. Rev. Mol. Cell Biol. *21*, 678–695. https://doi.org/10.1038/s41580-020-0270-8.

51. Wang, Y., Gao, W., Shi, X., Ding, J., Liu, W., He, H., Wang, K., and Shao, F. (2017). Chemotherapy drugs induce pyroptosis through caspase-3 cleavage of a gasdermin. Nature *547*, 99–103. https://doi.org/10.1038/nature22393.

52. Liu, Z., Wang, C., Yang, J., Zhou, B., Yang, R., Ramachandran, R., Abbott, D.W., and Xiao, T.S. (2019). Crystal Structures of the Full-Length Murine and Human Gasdermin D Reveal Mechanisms of Autoinhibition, Lipid Binding, and Oligomerization. Immunity *51*, 43–49.e44. https://doi.org/10.1016/j.immuni.2019.04.017.

53. E, K. (2001). The serum levels of IL-12 and IL-16 in cancer patients. Relation to the tumour stage and previous therapy. Biomed. Pharmacother. *55*, 111–116. https://doi.org/10.1016/s0753-3322(00)00023-8.

54. ElAtta, A.A., Ali, Y., Bassyouni, I., and Talaat, R. (2019). Correlation of myomir-206 and proinflammatory cytokines (IL-16 and IL-17) in patients with rheumatoid arthritis. Reumatologia *57*, 72–77. https://doi.org/10.5114/reum.2019.84811.

55. Folkersen, L., Gustafsson, S., Wang, Q., Hansen, D.H., Hedman, Å.K., Schork, A., Page, K., Zhernakova, D.V., Wu, Y., Peters, J., et al. (2020). Genomic and drug target evaluation of 90 cardiovascular proteins in 30,931 individuals. Nat. Metab. *2*, 1135–1148. https://doi.org/10.1038/s42255-020-00287-2.

56. Zhang, J., Yang, Z., Liang, Z., Wang, M., Hu, C., Chang, C., Shi, L., Ji, Q., and Liu, L. (2021). Anti-Interleukin-16-Neutralizing Antibody Attenuates Cardiac Inflammation and Protects against Cardiac Injury in Doxorubicin-Treated Mice. Mediators Inflamm. *2021*, 6611085. https://doi.org/10.1155/2021/6611085.

57. Kvaskoff, M., Mu, F., Terry, K.L., Harris, H.R., Poole, E.M., Farland, L., and Missmer, S.A. (2015). Endometriosis: a high-risk population for major chronic diseases? Hum. Reprod. Update *21*, 500–516. https://doi.org/10.1093/humupd/dmv013.

58. Bulun, S.E., Yilmaz, B.D., Sison, C., Miyazaki, K., Bernardi, L., Liu, S., Kohlmeier, A., Yin, P., Milad, M., and Wei, J. (2019). Endometriosis. Endocr. Rev. *40*, 1048–1079. https://doi.org/10.1210/er.2018-00242.

59. Taylor, H.S., Kotlyar, A.M., and Flores, V.A. (2021). Endometriosis is a chronic systemic disease: clinical challenges and novel innovations. Lancet *397*, 839–852. https://doi.org/10.1016/s0140-6736(21)00389-5.

60. Guo, M., Bafligil, C., Tapmeier, T., Hubbard, C., Manek, S., Shang, C., Martinez, F.O., Schmidt, N., Obendorf, M., Hess-Stumpp, H., et al. (2020). Mass cytometry analysis reveals a distinct immune environment in peritoneal fluid in endometriosis: a characterisation study. BMC Med. *18*, 3. https://doi.org/10.1186/s12916-019-1470-y.

61. Xiao, F., Liu, X., and Guo, S.W. (2020). Platelets and Regulatory T Cells May Induce a Type 2 Immunity That Is Conducive to the Progression and Fibrogenesis of Endometriosis. Front. Immunol. *11*, 610963. https://doi.org/10.3389/fimmu.2020.610963.

62. Tan, Y., Flynn, W.F., Sivajothi, S., Luo, D., Bozal, S.B., Davé, M., Luciano, A.A., Robson, P., Luciano, D.E., and Courtois, E.T. (2022). Single-cell analysis of endometriosis reveals a coordinated transcriptional programme driving immunotolerance and angiogenesis across eutopic and ectopic tissues. Nat. Cell Biol. *24*, 1306–1318. https://doi.org/10.1038/s41556-022-00961-5.

63. Olive, D.L. (2008). Gonadotropin-releasing hormone agonists for endometriosis. N. Engl. J. Med. *359*, 1136–1142. https://doi.org/10.1056/NEJMct0803719.

64. Hidari, T., Hirata, T., Arakawa, T., Koga, K., Neriishi, K., Fukuda, S., Nakazawa, A., Nagashima, N., Ma, S., Sun, H., et al. (2019). Contralateral ovarian endometrioma recurrence after unilateral salpingo-oophorectomy. BMC Wom. Health *19*, 59. https://doi.org/10.1186/s12905-019-0760-z.

65. Chantalat, E., Valera, M.C., Vaysse, C., Noirrit, E., Rusidze, M., Weyl, A., Vergriete, K., Buscail, E., Lluel, P., Fontaine, C., et al. (2020). Estrogen Receptors and Endometriosis. Int. J. Mol. Sci. *21*, 2815. https://doi.org/10.3390/ijms21082815.

66. Zhao, Y., Gong, P., Chen, Y., Nwachukwu, J.C., Srinivasan, S., Ko, C., Bagchi, M.K., Taylor, R.N., Korach, K.S., Nettles, K.W., et al. (2015). Dual suppression of estrogenic and inflammatory activities for targeting of endometriosis. Sci. Transl. Med. *7*, 271ra9. https://doi.org/10.1126/scitranslmed.3010626.

67. Van Langendonckt, A., Casanas-Roux, F., and Donnez, J. (2002). Iron overload in the peritoneal cavity of women with pelvic endometriosis. Fertil. Steril. *78*, 712–718.

68. Arumugam, K., and Yip, Y.C. (1995). De novo formation of adhesions in endometriosis: the role of iron and free radical reactions. Fertil. Steril. *64*, 62–64. https://doi.org/10.1016/S0015-0282(16)57655-9.

69. Defrère, S., Van Langendonckt, A., Vaesen, S., Jouret, M., González Ramos, R., Gonzalez, D., and Donnez, J. (2006). Iron overload enhances epithelial cell proliferation in endometriotic lesions induced in a murine model. Hum. Reprod. *21*, 2810–2816. https://doi.org/10.1093/humrep/del261.

70. Nakamura, T., Naguro, I., and Ichijo, H. (2019). Iron homeostasis and iron-regulated ROS in cell death, senescence and human diseases. Biochim. Biophys. Acta. Gen. Subj. *1863*, 1398–1409. https://doi.org/10.1016/j.bbagen.2019.06.010.

71. Arumugam, K. (1994). Endometriosis: Endometriosis and infertility: raised iron concentration in the peritoneal fluid and its effect on the acrosome reaction. Hum. Reprod. *9*, 1153–1157. https://doi.org/10.1093/oxfordjournals.humrep.a138649.

STAR★METHODS

KEY RESOURCES TABLE

REAGENT or RESOURCE	SOURCE	IDENTIFIER
Antibodies		
Anti-Human CD3 FITC (clone UCHT1)	BD Bioscience	Cat# 555332; RRID: AB_395739
Anti-Human CD3 BV605 (clone SK7)	Biolegend	Cat# 344836; RRID:AB_2565825
Anti-Human CD3 PerCP-Cy5.5 (clone HIT3a)	Biolegend	Cat# 300328; RRID:AB_1575008
Anti-Human CD3 APC-Cy7 (clone SK7)	Biolegend	Cat# 344818; RRID:AB_10645474
Anti-Human CD4 FITC (clone RPA-T4)	Biolegend	Cat# 300506; RRID:AB_314074
Anti-Human CD4 PerCP-Cy5.5 (clone RPA-T4)	BD Bioscience	Cat# 560650; RRID: AB_1727476
Anti-Human CD4 BV605 (clone RPA-T4)	Biolegend	Cat# 317438; RRID:AB_11218995
Anti-Human CD56 FITC (clone B159)	BD Bioscience	Cat# 557699; RRID:AB_396808
Anti-Human CD56 APC (clone B159)	BD Bioscience	Cat# 557711; RRID:AB_396820
Anti-Human CD56 BV421 (clone HCD56)	Biolegend	Cat# 318328; RRID:AB_11218798
Anti-Human CD56 BV510 (clone HCD56)	Biolegend	Cat# 318340; RRID:AB_2561944
Anti-Human CD8 PE-CY7 (clone RPA-T8)	BD Bioscience	Cat# 557746; RRID:AB_396852
Anti-Human CD163 BV421 (clone GHI/61)	Biolegend	Cat# 333612; RRID:AB_2562463
Anti-Human IL-6 PE (clone MQ2-13A5)	Biolegend	Cat# 501106; RRID:AB_315154
Anti-Human IL-8 PE (clone G265-8)	BD Bioscience	Cat# 554720; RRID:AB_395529
Anti-Human IL-16 PE (clone 14.1)	Biolegend	Cat# 519106; RRID:AB_10897940
Anti-Human TNF PE (clone MAb11)	BD Bioscience	Cat# 559321; RRID:AB_397219
Anti-Human Granzyme B APC (clone GB11)	Biolegend	Cat# 515406; RRID:AB_2566333
Anti-Human Active caspase3 FITC (clone C92-605)	BD Bioscience	Cat# 560901; RRID:AB_10563896
Anti-Human GSDME PE (clone EPR19859)	Abcam	Cat# ab225520; RRID:AB_3075533
Anti-Human TGF-β1 BV421 (clone TW4-2F8)	Biolegend	Cat# 349613; RRID:AB_10897450
Anti-Human CD45 BV510 (clone HI30)	BD Bioscience	Cat# 563204; RRID:AB_2738067
Anti-Human CD45 PerCP-Cy5.5 (clone 2D1)	Biolegend	Cat# 368504; RRID:AB_2566352
Anti-Human CD45 APC (clone HI30)	BD Bioscience	Cat# 555485; RRID:AB_398600
Anti-Human GSDME (clone EPR19859)	Abcam	Cat# ab215191; RRID:AB_2737000
Anti-Human GSDME (Polyclonal)	Abcam	Cat# ab230482; RRID:AB_3075534
Anti-Human Ferritin (clone EPR3004Y)	Abcam	Cat# ab75973; RRID:AB_1310222
Anti-Human Caspas3 p12 (clone EPR16888)	Abcam	Cat# ab179517; RRID:AB_2893359
Anti-Human IL-16 (clone EPR19988)	Abcam	ab207181; RRID:AB_3075535
Anti-Human IL-6 (Polyclonal)	Abcam	Cat# ab6672; RRID:AB_2127460
Anti-Human CD45 (clone D3F8Q)	Cell Signaling Technology	Cat# 70257; RRID:AB_2799780
Anti-Human CD56 (clone 123C3)	Cell Signaling Technology	Cat# 3576; RRID:AB_2149540
Anti-Human CD163 (clone EPR19518)	Abcam	Cat# ab182422; RRID:AB_2753196
Anti-Human CD4 (clone EPR6855)	Abcam	Cat# ab133616; RRID:AB_2750883
Anti-Human CD8 (clone C8/144B)	Abcam	Cat# ab17147; RRID:AB_443686
Anti-Human CD14 (clone D7A2T)	Cell Signaling Technology	Cat# 75181; RRID:AB_2799865
Anti-Human CD19 (clone D4V4B)	Cell Signaling Technology	Cat# 90176; RRID:AB_2800152
Anti-rabbit IgG, HRP-linked	Cell Signaling Technology	Cat# 7074; RRID:AB_2099233

(*Continued on next page*)

Continued

REAGENT or RESOURCE	SOURCE	IDENTIFIER
Anti-mouse IgG, HRP-linked	Cell Signaling Technology	Cat# 7076; RRID:AB_330924
Biological samples		
Relatively normal endometrium (RNE) tissue was scraped from surgically discarded tissue from patients with uterine fibroids who underwent a total hysterectomy	The First Affiliated Hospital of the University of Science and Technology of China	Ethics Number: 2019-ky066
Ectopic endometrium(EE) tissue is obtained from surgically discarded tissue from patients with ovarian endometriosis	The First Affiliated Hospital of the University of Science and Technology of China	Ethics Number: 2019-ky066
Chemicals, peptides, and recombinant proteins		
Alexa Fluor™488 Tyramine SuperBoost™ Kit (Goat Anti-Mouse IgG)	Thermo Fisher Scientific	B40912
Alexa Fluor™488 Tyramine SuperBoost™ Kit (Goat Anti- Rabbit IgG)	Thermo Fisher Scientific	B40922
Alexa Fluor™555 Tyramine SuperBoost™ Kit (Goat Anti-Rabbit IgG)	Thermo Fisher Scientific	B40923
Alexa Fluor™555 Tyramine SuperBoost™ Kit (Goat Anti-Mouse IgG)	Thermo Fisher Scientific	B40913
Alexa Fluor™647 Tyramine SuperBoost™ Kit (Goat Anti-Mouse IgG)	Thermo Fisher Scientific	B40916
Alexa Fluor™647 Tyramine SuperBoost™ Kit (Goat Anti-Rabbit IgG)	Thermo Fisher Scientific	B40926
T-PER Tissue Protein Extraction Reagent	Thermo Fisher Scientific	78510
TRIzol™ Reagent	Thermo Fisher Scientific	15596018
SYBR® Green Premix Pro Taq HS qPCR Kit II	Accurate Biology	AG11702
Prime Script RT reagent Kit with gDNA Eraser	Takara	RR047A
SuperSignal™ West Atto Ultimate Sensitivity Substrate	Thermo Fisher Scientific	A38555
SuperSignal™ West Femto Sensitivity Substrate	Thermo Fisher Scientific	34094
Pierce™ BCA Protein Assay Kits	Thermo Fisher Scientific	23227
Deferoxamine mesylate (DFO)	Selleck	S5742
Z-DEVD-FMK	Selleck	S7312
BODIPY™ 581/591 C11	Thermo Fisher Scientific	D3861
Lipid Peroxidation (MDA) Assay Kit	Abcam	ab118970
Iron–Dextran	Sigma	D8517
Z30702029	Enamine	Z30702029
Z1139266079	Enamine	Z1139266079
Z2600845982	Enamine	Z2600845982
Zombie NIR	Biolegend	423106
DAPI	Biolegend	422801
Recombinant Human IL-16 Protein	R&D	316-IL-025
Recombinant Human IL-6 Protein	Peprotech	200–06
Critical commercial assays		
Fixation/Permeabilization Solution Kit	BD Bioscience	Cat# 554714
eBioscience™ Foxp3/Transcription Factor Staining Buffer Set	eBioscience	Cat# 00-5523-00
Hu IL-6 CBA Flex Set A7 100Tst	BD	558276
Hu IL-8 CBA Flex Set A9 100Tst	BD	558277
Hu TNF CBA Flex Set D9 100Tst	BD	558273

(*Continued on next page*)

Continued

REAGENT or RESOURCE	SOURCE	IDENTIFIER
Hu IL-1Bta CBA Flex Set B4 100Tst	BD	558279
Hu TGF-Bta1 CBA Flex Set B6 100Tst	BD	560429
Hu Solbl Ptein CBA Buf Kit 100Tst	BD	558264
Human IL-1β ELISA Kit	Dakewe Bio	1110122
Human IL-6 ELISA Kit	Dakewe Bio	1110602
Human IL-8 ELISA Kit	Dakewe Bio	1110802
Human IL-16 ELISA Kit	LiankeBio	70-EK116-96
Human Ferritin ELISA Kit	Abcam	ab108837
Collagenase Type IV	sigma	C5138
DNase I	sigma	11284932001
TMRM	sigma	T5428
MitoTracker	Thermo	M7514
Deposited data		
scRNA sequencing data	This paper	GEO: GSE229735
Experimental models: Cell lines		
293T	ATCC	CRL-3216
Jurkat	ATCC	TIB-152
Experimental models: Organisms/strains		
Mouse: C57BL/6JGpt	GemPharmatech	Strain no. N000013
Mouse: B6/JGpt-Il16em7Cd2318in6/Gpt	GemPharmatech	Strain NO.T007605
Oligonucleotides		
qPCR primers for various genes	This paper	Table S2
PCR primers for Mouse genotype	This paper	Table S3
Software and algorithms		
FlowJo software version 10.6.2	FlowJo, LLC	https://www.flowjo.com/
Prism version 8	Graphpad	https://www.graphpad.com/
Image Lab 5.2.1	Image Lab	https://www.bio-rad.com/en-hk/product/image-lab-software?ID=KRE6P5E8Z
R 4.2.2	R	https://cran.r-project.org/

RESOURCE AVAILABILITY

Lead contact

Further information and requests for resources and reagents should be directed to and will be fulfilled by the lead contact Haiming Wei. (ustcwhm@ustc.edu.cn).

Materials availability

This study did not generate new unique reagents or materials.

Data and code availability

- All data required to understand and evaluate the conclusions of this paper are provided in the manuscript and supplementary materials. Raw sequencing data can be accessed from the Gene Expression Omnibus (GEO) database:GSE229735.
- This paper does not report any original code.
- Any additional information required to reanalyze the data reported in this work paper is available from the lead contact upon request.

EXPERIMENTAL MODEL AND STUDY PARTICIPANT DETAILS

Human subjects

Ectopic endometrial tissue (n = 140) was acquired from women aged 32.13 ± 6.21 years who had undergone surgery for endometriosis. Relatively normal endometrial tissue (n = 68) was acquired from women aged 47.02 ± 3.95 years who had undergone surgery

for uterine fibroids. All relatively normal endometrial tissues were examined by experienced obstetrician-gynecologists during surgery and possessed no significant abnormalities. All women who donated tissue were premenopausal and had not been administered hormone or anticoagulant therapy in the preceding six months. Ethical approval has been obtained from the First Affiliated Hospital of the University of Science and Technology of China (Ethics Number: 2019-ky066), including procedures for informing patients or their family members and obtaining their consent. The clinical data for the endometriosis patients and controls are outlined in Table S1. More detail information of patients can be found in Table S4.

Mice

The IL16 knockout mice were purchased from GemPharmatech (Strain no.T007605). This mouse line represented a whole-body knockout, in which IL16 is deleted in all cell types. The genotype identification primers can be found in Table S3, and the knockout strategy utilized in this study is outlined in Figure S3. For our experiments, 8 to 12-week-old female mice in a C57BL/6 background were used. Mice were maintained under specific pathogen-free (SPF) conditions with a strict 12-h light cycle (lights on at 08:00 and off at 20:00). All animal studies were conducted according to protocols approved by the Ethics Committee of the University of Science and Technology of China (USTCACUC1801018).

Human sample isolation

Fresh specimens were rinsed and homogenized into small pieces with a diameter of less than 2 mm. Lymphocytes were extracted from ectopic endometrial tissue samples by digesting the tissues with 5 mg/mL collagenase type IV (C5138, Sigma, USA) for 40 min at 37°C. Lymphocytes were extracted from normal endometrial tissue samples by digesting the tissues with 2 mg/mL collagenase type IV for 40 min at 37°C. The suspensions were strained through a 100-μm nylon cell strainer (431752, Corning, USA). The lymphocytes were then immediately analyzed using flow cytometry.

Surgically induced endometriosis

Endometriosis in mice was surgically induced under aseptic conditions and anesthesia. Specifically, on day 1, mice were subjected to ovariectomy at the age of six weeks; on day 7, ovariectomized mice were implanted with a sterile, 60-day release pellet containing 0.36 mg of 17-β estradiol (Innovative Research of America, Sarasota, FL, USA). On day 9, one uterine horn of a donor mouse was extracted under anesthesia. In a Petri dish containing warmed 1640 medium supplemented with 100 U/mL penicillin and 100 μg/mL streptomycin, uterine horns were longitudinally sectioned with scissors. Next, using a 2 mm dermal biopsy punch, one endometrial fragment was isolated and sutured to the mesenteric membrane of the recipient mouse intestine via a midline incision (6-0 braided polypropylene suture). In sham-treated control mice, a suture was performed without using endometrial tissue fragments. The abdominal incision was closed with a 3-0 braided polypropylene suture continuously. On day 30, after endometriosis was induced, the mice were sacrificed, and the endometriotic lesions and ectopic endometria were carefully removed from the surrounding tissue. For the experiments using Z30702029 to treat the endometriosis mouse model, following the implantation of the endometrial tissues, we administered intraperitoneal injections of 200 μL of PBS twice per week to the control group mice and intraperitoneal injections of Z30702029 at a dosage of 15 mg/kg twice per week to the treatment group mice.

METHOD DETAILS

The Von Frey filament test

The pain threshold of the mice was characterized using a previously described method with slight modifications (Zhu et al., 2021). The mechanical withdrawal threshold was assessed using Von Frey filaments placed on the middle of the plantar surface of the left hind paw. Mice were individually situated in transparent plastic chambers on a wire mesh grid. Following acclimatization to the test environment for 30 min, a filament probe was inserted, and the pressure was gradually increased. A response was considered positive when a mouse withdrew or licked its paw. The withdrawal threshold was calculated as the average of five applications.

Quantitative PCR analysis of ferritin heavy chain (FTH)1 and GPX4 expression

To contrast the expression of *FTH1* and *GPX4* in T cells from normal and ectopic endometria, total RNA was extracted using TRIzol (15596018, Thermo Fisher Scientific, USA) and reverse-transcribed using the PrimeScript RT Reagent Kit with gDNA Eraser (RR047A, Takara, Japan). The resulting cDNA was examined for the expression of the *FTH1* and *GPX4* genes using qPCR with TB Green Premix Ex Taq (RR820A, Takara). The primers utilized are listed in Table S2.

Histological analyses

Specimens were fixed in 10% neutral formaldehyde and embedded in paraffin wax. Paraffin-embedded tissues were sectioned into 3 μm slices, dewaxed and rehydrated utilizing standard procedures, and stained with hematoxylin and eosin (H&E), Sirius red, Masson stain, or Prussian blue.

Immunohistochemistry (IHC)

IHC was conducted following the blocking of the endogenous peroxidase activity. Specifically, the antigen was retrieved using a Tris-EDTA solution (pH 9.0) followed by blocking with 10% normal goat serum. Sections were incubated with primary antibodies at 4°C overnight. After incubation with a SPlink Detection Kit (SP-9001 or SP-9002, ZSGB-BIO, Beijing, China), immunoreactivity was characterized using a DAB Substrate Kit (8059, Cell Signaling Technology, USA). This was followed by hematoxylin staining. Ultimately, the sections were dehydrated, hyalinized, and cover-slipped. The primary antibodies utilized are outlined in the key resources table.

Multiplex immunohistochemistry (mIHC)

mIHC was conducted using sequential staining cycles. In particular, formalin-fixed, paraffin-embedded sections were deparaffinized, and the antigen was retrieved in a Tris–EDTA solution (pH 9.0) using a microwave. Following blocking, the sections were incubated with primary antibodies at 4°C overnight and treated with a poly-HRP-conjugated secondary antibody (Thermo Fisher Scientific) at room temperature for 1 h. Tyramide signal amplification (TSA) was conducted using an Alexa Fluor Tyramide SuperBoost Kit (Thermo Fisher Scientific). Following each staining cycle, the samples were heated in a microwave to remove the antibody-TSA complex. After all cycles had been completed, the sections were counterstained using DAPI. Images were captured using an LSM 880 inverted confocal laser scanning microscope with Airyscan (Zeiss, Oberkochen, Germany). The primary antibodies used are listed in the key resources table.

Immunofluorescence

T cells extracted from normal or ectopic endometrium were fixed in 4% paraformaldehyde (PFA) at room temperature (RT) for 15 min and rinsed three times with phosphate-buffered saline (PBS) supplemented with 0.1% bovine serum albumin (BSA). Immunofluorescence staining was conducted using a standard protocol as follows. Samples were incubated in blocking buffer (5% normal goat serum, 0.5% Triton X-100 in PBS) at RT for 1 h and then with primary antibodies at 4°C overnight. The samples were incubated with Alexa Fluor 488-conjugated goat anti-rabbit IgG (A-11008, Thermo Fisher Scientific) and Alexa Fluor 546-conjugated goat anti-mouse IgG (A-11030, Thermo Fisher Scientific) for 1 h. Images were obtained using an LSM 880 inverted confocal laser scanning microscope with an Airyscan detector (Zeiss). The primary antibodies utilized are listed in the key resources table.

Scanning electron microscopy (SEM)

Jurkat cells were incubated with iron dextran (25 μL/mL) or PBS for 24 h and then collected. Images of the cell surface were acquired using an SU8100 SEM (Hitachi, Japan).

Antibody array

Cystic fluid was obtained from three endometriosis patients. The levels of various cytokines were examined using the G-Series Human Cytokine Antibody Array Kit (RayBiotech, USA), following the manufacturer's directions. Specifically, the glass slide was thoroughly air-dried and blocked. Samples were added to the glass slide and incubated at 4°C overnight. The glass slide was then incubated with a biotinylated antibody cocktail and cy3 equivalent dye-streptavidin. The signal was detected using an InnoScan 300 Microarray Scanner (Innopsys, Carbonne, France). Data were analyzed utilizing GSH-CAA-440 software (RayBiotech).

Flow cytometry

Cells were diluted 1:100 in PBS. For intracellular cytokine staining, the cells were incubated with phorbol myristate acetate (PMA, 50 ng/mL), ionomycin (1 μg/mL), and monensin (10 μg/mL) for 4 h, collected for surface staining and treated with permeabilization buffer from the Foxp3 transcription factor staining buffer set (eBioscience, San Diego, CA, USA) based on the manufacturer's instructions. Flow cytometry was conducted using an LSR II flow cytometer (BD Biosciences, Franklin Lakes, NJ, USA) according to the manufacturer's directions. Data were examined using FlowJo vX.0.7 software (BD Biosciences). The flow cytometry antibodies utilized are listed in the key resources table.

Cell sorting using flow cytometry (flow sorting)

T cells were stained using cell fluorochrome-conjugated antibodies against CD45 (368504, Biolegend, USA), Zombie NIR (423106, BioLegend), CD3 (555332, BD Biosciences), and CD56 (557711, BD Biosciences), before sorting. The $CD45^{+}NIR^{-}CD3^{+}CD56^{-}$ T cells were detected and collected using a FACS Aria flow cytometer (BD Biosciences).

The enzyme-linked immunosorbent assay (ELISA)

ELISA kits were employed to detect IL-1β (1110122, Dakewe Biotech, China), IL-6 (1110602, Dakewe Biotech), IL-8 (1110802, Dakewe Biotech), active IL-16 (70-EK116-96, LiankeBio, USA), and ferritin (ab108837, Abcam, UK) in cystic fluid, based on the manufacturer's instructions.

Cytometric bead array (CBA) assay

Cytokines (IL-1β, IL-6, IL-8, TNF, and TGF-β) in PBMC cell culture supernatants were identified using the CBA assay. The specific kits employed in this assay are listed in the key resources table. All assays followed the manufacturer's instructions, and samples were quantified using a BD Biosciences LSR II flow cytometer. Data were analyzed using FlowJo vX.0.7 software (BD Biosciences).

Western blot analysis

Total protein was extracted from cells using RIPA lysis buffer (89900, Thermo Fisher Scientific). Protein concentrations were characterized using the Pierce BCA Protein Assay Kit (23225, Thermo Fisher Scientific). Equal protein concentrations were separated through SDS-PAGE and transferred to polyvinylidene difluoride (PVDF) membranes. PVDF membranes were blocked using 5% dry skimmed milk in Tris-buffered saline-1% Tween (TBST) for 30 min and incubated with primary antibodies overnight at 4°C. Blots were incubated with HRP-conjugated anti-rabbit (7074S, Cell Signaling Technology) or anti-mouse (7076S, Cell Signaling Technology) antibodies for 1 h. Bands were detected using the SuperSignal West Femto Maximum Sensitivity Substrate (34094, Thermo Fisher Scientific). Membranes were rinsed with neutral antibody stripping buffer (Beyotime, China) to remove the antibodies for reuse. The antibodies used for western blotting are listed in the key resources table. The original WB image can be found in Figure S8.

Droplet-based scRNA-seq (10x chromium)

scRNA-seq was conducted by Genergy Bio-Technology Co., Ltd. (Shanghai, China). Specifically, a pure population of $CD45^+$ cells (from normal or ectopic endometrial samples) were acquired via sorting on a flow cytometer and then loaded onto a 10x Chromium microfluidics system (10x Genomics, San Francisco, USA) following the manufacturer's guidelines. Libraries were constructed using the Single Cell 3′ library and Gel Bead Kit v.3 (10x Genomics) based on the manufacturer's guidelines. The prepared library pools were sequenced on an Illumina Novo 6000 platform (Illumina, USA) with 150-bp paired-end reads.

10x scRNA-seq data processing

The raw reads from droplet-based scRNA-seq by 10x Chromium were aligned to the human reference genome (GRCh38) utilizing the CellRanger toolkit (version 3.1.0, https://github.com/10XGenomics/cellranger) and default parameters. UMI count matrices from patients and controls were imported and merged using the Seurat package (version 3.2.0, http://satijalab.org/seurat/) for preprocessing, clustering analysis, and visualization. Low-quality samples with fewer than 500 cells or if the percentage of mitochondrial UMIs was >10% were removed. In total, 11,250 cells were retained for further analysis (normal endometrium, 5,737 cells; ectopic endometrium, 5,521 cells).

Data integration and cell type annotation

UMI matrices from various samples were integrated, log-normalized with log(CPM/100 + 1), and scaled using the top 2000 highly variable genes for dimensionality reduction through principal component analysis (PCA). The merged dataset was integrated using the 'harmony' algorithm using the RunHarmony function in Seurat. Graph-based clustering and *t*-distributed stochastic neighbor embedding (tSNE) were conducted on the first 15 harmony embeddings using the FindNeighbors, FindClusters, and RunTSNE functions alongside default parameters. We characterized ten major cell clusters based on canonical markers.

Lactate dehydrogenase (LDH) assay

Cell culture supernatant (50 μL) was transferred to a 96-well plate. Cytotoxicity was characterized using the CyQUANT LDH Cytotoxicity Assay (C20301, Thermo Fisher Scientific) following the manufacturer's instructions.

Lipid peroxidation assay

Freshly extracted normal and ectopic endometrial cells were resuspended in complete medium. Following centrifugation at 350 × g for 10 min, the cells were incubated with a final concentration of 0.02 μg/μL phycoerythrin (PE)-conjugated mouse anti-chicken macrophage-monocyte (Southern Biotech, Birmingham, AL, USA) monoclonal antibody in the dark for 30 min on ice. Lipid peroxidation was examined using a lipid peroxidation kit (ab243377, Abcam) or BODIPY 581/591 C11 (D3861, Thermo Fisher Scientific) according to the manufacturer's instructions. Specifically, a lipid peroxidation sensor was included with freshly isolated normal and ectopic endometrial cells for 30 min and employed for flow cytometry staining. Following rinsing with HBSS, flow analyses were conducted on a BD Biosciences LSR II flow cytometer. The fluorescein isothiocyanate (FITC)/PE ratio was employed to assess lipid peroxidation levels in various cell types.

Iron detection assay

Levels of Fe^{2+} in serum and cystic fluid samples were characterized using an iron assay kit (MAK025, Sigma-Aldrich) according to the manufacturer's protocol.

QUANTIFICATION AND STATISTICAL ANALYSIS

Statistical analysis was conducted using Prism 8 software (GraphPad, USA). Paired or unpaired two-tailed *t*-tests were employed to determine statistical significance. The specific statistical parameters are denoted in the legend of each figure.